1

Solid State Research

1970

Prepared under Electronic Systems Division Contract AF 19(628)-5167 by

Lincoln Laboratory

MASSACHUSETTS INSTITUTE OF TECHNOLOGY

Lexington, Massachusetts

1

Solid State Research

1970

Issued 6 May 1970

Prepared under Electronic Systems Division Contract AF 19(628)-5167 by

Lincoln Laboratory

MASSACHUSETTS INSTITUTE OF TECHNOLOGY

Lexington, Massachusetts

The work reported in this document was performed at Lincoln Laboratory, a center for research operated by Massachusetts Institute of Technology, with the support of the Department of the Air Force under Contract AF 19(628)-5167.

ABSTRACT

This report covers in detail the solid state research work at Lincoln Laboratory for the period 1 November 1969 through 31 January 1970. The topics covered are Solid State Device Research, Materials Research, and Physics of Solids.

Accepted for the Air Force
Franklin C. Hudson
Chief, Lincoln Laboratory Office

INTRODUCTION

I. SOLID STATE DEVICE RESEARCH

Single mode CW laser emission has been obtained at 12°K from a $Pb_{0.685}Sn_{0.315}Te$ diode at 31.8 μ. This is the longest wavelength semiconductor laser emission observed to date in the absence of a magnetic field. In addition, $Pb_{1-x}Sn_xTe$ diode lasers have been fabricated with threshold current densities as low as 20 amp/cm^2. To our knowledge, this is the lowest value ever observed for a semiconductor laser.

In continuing the study of the materials and electrical properties of $Pb_{1-x}Sn_xTe$ alloys, we have determined the Hall coefficient and electrical resistivity at 4.2°K of several samples with x up to 0.3. Mobilities as high as 5.4×10^5 cm^2/V-sec have been observed for x = 0.2 with an n-type carrier concentration of 1.8×10^{17} cm^{-3}. Although the mobilities remain high in the alloy system, there is a trend toward lower values at higher Sn content.

$Pb_{1-x}Sn_xTe$ diode lasers have also been fabricated using evaporated Schottky barrier metal contacts instead of conventional p-n junctions. Metals such as Pb, In, Zn and Sn with small work functions produce a narrow n-type degenerate inverted layer on the surface of p-type samples. When the diodes are forward biased, electrons are injected from the inverted layer into the bulk. Low threshold diode lasers have been fabricated in this fashion from p-type PbTe with emission at 6.4 μ and $Pb_{0.8}Sn_{0.2}Te$ with emission at 15 μ. Barriers have been observed on very narrow gap alloys of $Pb_{1-x}Sn_xTe$, and work is continuing to determine the maximum laser wavelength which can be obtained.

The amplification of 2.3-GHz acoustic waves in GaAs at room temperature has been observed using Brillouin scattering techniques. The amplification occurs through the piezoelectric interaction between the shear acoustic waves and electrons drifting under the application of an external electric field. The observed gain of 0.16 dB/V is in good agreement with theoretical predictions.

The temperature and impurity concentration dependence of the electron mobility in high purity GaAs has been determined. Adjustment of the conduction band deformation potential to 7.0 eV results in excellent agreement between experiment and a theory combining polar optical phonon, piezoelectric acoustic phonon, deformation potential acoustic phonon, ionized impurity and neutral impurity scattering in the relaxation time approximation. Experimental 77°K mobilities of 210,000 cm^2/V-sec are very close to the calculated lattice limited mobility of 240,000 cm^2/V-sec.

Room temperature electrical resistivity of EuO is reported as a function of pressure up to 10 kbar. For the higher resistivity samples, the pressure coefficient corresponds very closely to the observed shift of the optical absorption edge with pressure. Both the temperature and pressure dependence of the electrical resistivity are explained in terms of a model in which electrons are distributed between a temperature and pressure sensitive conduction band and a localized stationary trap level.

II. MATERIALS RESEARCH

The phase diagram of the PbTe-PbSe pseudobinary system has been determined by thermal analysis. The relationship between the liquidus and solidus temperatures, both of which increase monotonically and sublinearly with increasing PbSe content, is given by the ideal form of the liquidus-solidus equation for binary alloy systems.

The composition stability limits of $(Pb_{1-y}Sn_y)_{1-x}Te_x$ alloys with y = 1.0, 0.9, and 0.8 have been determined by using x-ray diffraction analysis to measure the lattice parameters of annealed powder samples as a function of x, the atom fraction of Te. The metal-rich stability limit at 400°C is x = 0.5000 for all three values of y. The Te-rich limit at 350°C is x = 0.5070, 0.5058, and 0.5037 for y = 1.0, 0.9, and 0.8, respectively.

The pressure-composition phase diagram for the $Sr_{1-x}Pb_xRuO_3$ system at 1400°C has been determined by x-ray diffraction measurements on samples quenched to room temperature before releasing the pressure. The pyrochlore form of $PbRuO_3$(x = 1), which is stable at atmospheric pressure, transforms to the perovskite form at 90 kbar. The pressure required to stabilize the perovskite form decreases with decreasing x, and for $0 < x < 0.3$ this form is the stable phase at atmospheric pressure.

III. PHYSICS OF SOLIDS

Ti_2O_3, a room temperature semiconductor which undergoes a semiconductor-metal transition at 400°K, is being investigated by both optical reflectance and Raman scattering techniques. The reflectance measured in the photon energy range from 0.1 to 11.0 eV, only at room temperature so far, has been used in a Kramers-Kronig analysis to obtain the real and imaginary parts of the dielectric constant. The Raman spectrum, investigated from 1.7° to 800°K with an argon ion laser, indicates that all the Raman modes persist up to 800°K; this implies no change of crystal symmetry at the semiconductor-metal transition.

A study has been carried out of the optical properties of simple metals including many-body effects. Results indicate that the optical properties can be calculated without an accurate determination of the many-body contributions, provided the energy band structure is known from experimental measurements.

A review of surface plasmon excitations in electron tunneling, low energy electron diffraction (LEED) and photoemission indicates that the first technique, i.e., tunneling, provides a simple, sensitive probe for studying surface plasmon excitations. The latter two techniques suffer from complexity of the excitation mechanism; using the two-potential formula for scattering, a theory has been developed which gives quantitative support to the interpretation of structure in recent LEED and photoemission experiments performed elsewhere.

An expression has been derived for the electrical conductivity of a crystal described by the single band Hubbard model for the case of an energy bandwidth Δ that is narrow compared with the intra-atomic Coulomb repulsion U. For the half-filled band at zero temperature, the conductivity vanishes. For Li-doped NiO, only a negligibly small DC conductivity due to

the $3d^8$ band hole hopping is calculated. In another investigation of the Hubbard model, both in the exact treatment of the widely separated atomic limit ($U \rightarrow 0$) and in the thermal single determinant variational approximation for small Δ/U, it is concluded that a phase transition at $T_M \sim U/4k$, found by several different groups for small Δ/U using the thermal Hartree-Fock approximation, is entirely spurious.

The ground-state spin configuration in Cr_5S_6 has been calculated using the Heisenberg Hamiltonian and minimizing the energy by the generalized Luttinger-Tisza method. Parameter space maps have been constructed showing the various ground-state regions for particular sets of values for nearest-neighbor and next-nearest-neighbor interactions.

Two-magnon Raman scattering has been observed from the two-dimensional antiferromagnet K_2NiF_4. The experimental results at low temperatures are consistent with a theoretical Green's function calculation of the Raman spectrum and give a nearest-neighbor intraplanar constant $J = 77.0 \pm 2.0\ cm^{-1}$, which is in good agreement with that obtained from one-magnon neutron scattering.

Raman scattering from optical phonons in $Hg_xCd_{1-x}Te$ has been investigated for the range $0 \leqslant x \leqslant 1$ between 1.7° and 300°K. The alloys exhibit scattering of a type II system where both the LO and TO phonons characteristic of pure CdTe and HgTe are present with an intensity proportional to alloy composition.

Raman scattering from single particle electron excitations gives a direct measure of the electron velocity distribution function. In GaAs the previous equilibrium distribution results have now been extended to the nonequilibrium case by studying the scattering from carriers subjected to high pulsed electric fields, up to the Gunn threshold.

The phenomenon of acoustical activity of transverse waves, predicted theoretically by Portigal and Burstein, has for the first time been directly observed in α-quartz with microwave ($\sim$1 GHz) shear waves propagating close to the optical axis. The magnitude of the activity is in good agreement with that calculated from our recent Brillouin scattering determination of the linear wave vector splitting of the two transverse acoustic normal modes.

CONTENTS

ORGANIZATION

SOLID STATE DIVISION

A. L. McWhorter, *Head*
P. E. Tannenwald, *Associate Head*
M. J. Hudson, *Assistant*
E. P. Warekois
C. R. Grant

SOLID STATE THEORY

H. J. Zeiger, *Leader*
M. M. Litvak, *Assistant Leader*

Bari, R. A.
Brine, N. S.
Chinn, S. R.*
Davies, R. W.
Dresselhaus, G. F.
Kaplan, T. A.
Kleiner, W. H.
Landon, S. N.
Larsen, D. M.
Ngai, K. L.
Palm, B. J.†
Wilson, A. R. M.
Young, C. Y.

SOLID STATE PHYSICS

J. G. Mavroides, *Leader*
G. B. Wright, *Assistant Leader*

Allen, J. W.
Barch, W. E.
Blum, F. A., Jr.
Brandt, R. C.
Burke, J. W.
Crooker, P. P.
DeFeo, W. E.
Dresselhaus, M. S.†
Dwight, K., Jr.
Feldman, B.
Fetterman, H.
Groves, S. H.
Henrich, V. E.
Johnson, E. J.
Kernan, W. C.
Kolesar, D. F.
Melngailis, J.
Menyuk, N.
Nill, K. W.
Parker, C. D.
Pine, A. S.
Scouler, W. J.
Waldman, J.*
Weber, R.

ELECTRONIC MATERIALS

J. B. Goodenough, *Leader*
A. J. Strauss, *Associate Leader*

Anderson, C. H., Jr.
Arnott, R. J.
Banus, M. D.
Batson, D. A.
Brebrick, R. F., Jr.
Button, M. J.
Capes, R. N., Jr.
Delaney, E. J.
England, R. E.
Fahey, R. E.
Finn, M. C.
Iseler, G. W.
Kafalas, J. A.
Kasper, H. M.
LaFleur, W. J.
Lavine, M. C.†
Longo, J. M.
Mastromattei, E. L.
O'Connor, J. R.
Owens, E. B.
Pierce, J. W.
Plonko, M. C.
Raccah, P. M.
Reed, T. B.
Roddy, J. T.
Searles, I. H.
Smith, F. T. J.
Stack, T. E.
Steininger, J. M.
Temkin, R. J.*

APPLIED PHYSICS

J. O. Dimmock, *Leader*
T. C. Harman, *Assistant Leader*
I. Melngailis, *Assistant Leader*

Brueck, S. R. J.*
Calawa, A. R.
Carter, F. B.
Caswell, F. H.
Clough, T. F.
Donnelly, J. P.
Ferrante, G. A.
Foyt, A. G.
Hurwitz, C. E.
Krohn, L., Jr.
Lindley, W. T.
Mooradian, A.
Murphy, R. A.*
Oliver, M. R.*
Orphanos, W. G.
Palmdino, A. E.
Rossi, J. A.
Spears, D. L.
Stillman, G. E.
Ward, J. H. R., III
Wolfe, C. M.
Woods, R. J.
Youtz, P.

* Research Assistant
† Part Time

REPORTS BY AUTHORS ENGAGED IN SOLID STATE RESEARCH

15 November 1969 through 15 January 1970

PUBLISHED REPORTS

Journal Articles*

JA No.			
3369	Inversion Asymmetry and Warping-Induced Interband Magneto-Optical Transitions in InSb	C. R. Pidgeon† S. H. Groves	Phys. Rev. 186, 824 (1969)
3423	Brillouin Scattering Study of Acoustic Attenuation in Fused Quartz	A. S. Pine	Phys. Rev. 185, 1187 (1969)
3444	Derivation of a Quasiparticle Transport Equation for an Impure Fermi Liquid at Low Temperatures	J. L. Sigel	Phys. Rev. 186, 182 (1969)
3483	X-Ray Diffraction Studies on Zn_3As_2 and Cd_3As_2 at High Pressure	M. D. Banus M. C. Lavine	High Temperatures-High Pressures 1, 269 (1969)
3485	Velocity and Attenuation of Hypersonic Waves in Liquid Nitrogen	A. S. Pine	J. Chem. Phys. 51, 5171 (1969)
3520	An On-Line Data Recording System	W. E. Krag N. L. Daggett R. N. Davis F. E. Perkins†	Rev. Sci. Instr. 40, 1606 (1969)
3525	Magnetic Ordering Effects in the Ultraviolet Reflectance of EuS and EuSe	W. J. Scouler J. Feinleib J. O. Dimmock C. R. Pidgeon†	Solid State Commun. 7, 1685 (1969)
3541	Magnetic Ordering Effects on the Reflectivity of EuS and EuSe	C. R. Pidgeon† J. Feinleib W. J. Scouler J. Hanus J. O. Dimmock T. B. Reed	Solid State Commun. 7, 1323 (1969)
3558	The Intensities of Spin Wave Resonance Modes in Thin Films	R. Weber P. E. Tannenwald C. H. Bajorek	Appl. Phys. Letters 16, 35 (1970)

* Reprints available.

† Author not at Lincoln Laboratory.

JA No.			
3585	Residual Impurities in High-Purity Epitaxial GaAs	C. M. Wolfe G. E. Stillman E. B. Owens	J. Electrochem. Soc. 117, 129 (1970)
3586	Optical Observation of Magnetic-Field-Induced Spin Alignment in Antiferromagnetic EuTe	J. Feinleib C. R. Pidgeon*	Phys. Rev. Letters 23, 1391 (1969)
3597	The Hubbard Model: Insulator or Conductor for Narrow Band Regime	R. A. Bari R. V. Lange*	Phys. Letters 30A, 418 (1969)
3612	Theory of Surface Plasmon Excitation in Low Energy Diffraction and in Photoemission	K. L. Ngai E. N. Economou* M. H. Cohen*	Phys. Rev. Letters 24, 61 (1970)
3624	Interstellar Masers	D. F. Dickinson* M. M. Litvak B. M. Zuckerman*	Sky and Telescope 39, 4 (1970)
MS-2389	Raman Scattering by Magnetic Excitations in $RbNiF_3$	S. R. Chinn H. J. Zeiger J. R. O'Connor	J. Appl. Phys. 40, 1603 (1969)
MS-2615	Magneto-Optics	J. G. Mavroides	Proceedings of International Conference on High Magnetic Fields and Their Applications, Nottingham, England, 17-19 September 1969, High Magnetic Fields and Their Applications, pp. 1-37 (1969)
MS-2623	Laser Beam Trapping and Non-Linear Interactions in Semiconductors	A. Mooradian	1969 NEREM Record 11, 44 (1969)

* * * * *

UNPUBLISHED REPORTS

Journal Articles

JA No.			
3551	Niobium Monoxide $3Nb + Nb_2O_5 \rightarrow 5NbO$	T. B. Reed E. R. Pollard* L. E. Lonney* R. E. Leohman* J. M. Honig*	Accepted by Inorg. Synth.

* Author not at Lincoln Laboratory.

JA No.			
3552	Resistivity, Magnetoresistance, and Hall Effect Studies in VO_x $(0.82 \leqslant x \leqslant 1.0)$	J. M. Honig* W. E. Wahnsiedler* M. D. Banus T. B. Reed	Accepted by J. Solid State Chem.
3557	Hall Coefficient Factor for Polar Mode Scattering in n-Type Gas	G. E. Stillman C. M. Wolfe J. O. Dimmock	Accepted by J. Phys. Chem. Solids
3563	Interdiffusion in Lead Selenide	R. W. Brodersen* J. N. Walpole* A. R. Calawa	Accepted by J. Appl. Phys.
3568	Atom Movements: Diffusion	R. F. Brebrick	Physics & Chemistry of Solids: An Introduction ed. by P. F. Weller (M. Dekker, Inc., N.Y.)
3577	Reinterpretation of $^4A_2 \rightarrow {}^2E$ Exciton Spectra in $YCrO_3$	J. W. Allen	Accepted by Solid State Commun.
3579	Photoluminescence Due to Isoelectronic Oxygen and Tellurium Traps in II-VI Alloys	G. W. Iseler A. J. Strauss	Accepted by J. Luminescence
3587	Split-Off Valence Band Parameters for GaAs from Stress-Modulated Magnetoreflectivity	M. Reine* R. L. Aggarwal* B. Lax* C. M. Wolfe	Accepted by Phys. Rev.
3590	Thermodynamics and Determination of the Liquidus-Solidus Gap in Homogeneous, Monotonic Alloy Systems	J. M. Steininger	Accepted by J. Appl. Phys.
3602	Laser Raman Spectroscopy	A. Mooradian	Accepted by Science
3606	High Temperature Electrical Properties of CdSe: Evidence for a Native Donor	F. T. J. Smith	Accepted by Solid State Commun.
3608	Vapor-Crystal Equilibrium and Electrical Properties of HgTe	A. J. Strauss R. F. Brebrick	Accepted by J. Phys. Chem. Solids
3610	Localized One-Electron States in Perfect Crystals As a Consequence of the Thermal Single Determinant Approximation	T. A. Kaplan P. N. Argyres*	Accepted by Phys. Rev.
3611	Magnetic Susceptibility of Europium Trifluoride	S. Kern* P. M. Raccah A. Tveten*	Accepted by J. Phys. Chem. Solids

* Author not at Lincoln Laboratory.

Reports

JA No.			
3620	Interband Magnetoreflection of α-Sn	S. H. Groves C. R. Pidgeon* A. W. Ewald* R. J. Wagner*	Accepted by J. Phys. Chem. Solids
3625	Report on the Symposium on Magnetic Semiconductors held in Yorktown Heights, N. Y., Nov. 1969	J. O. Dimmock	Accepted by Appl. Optics
3628	Electronic Structure of Palladium	F. M. Mueller* A. J. Freeman* J. O. Dimmock A. M. Furdyna*	Accepted by Phys. Rev.
3650	Pressure-Induced Pyrochlore to Perovskite Transformations in the $Sr_{1-x}Pb_xRuO_3$ System	J. A. Kafalas J. M. Longo	Accepted by Mat. Res. Bull.
MS-2677	Onset of Magnetism in Vanadium Oxides: ^{51}V NMR Studies of VO_x ($x = 0.86$ to 1.23)	W. W. Warren, Jr.* A. C. Gossard* M. D. Banus	Accepted by J. Appl. Phys.

Meeting Speeches†

MS No.			
2662	Two-Magnon Raman Scattering in $KNiF_3$	S. R. Chinn H. J. Zeiger J. R. O'Connor	15th Annual Conference on Magnetism and Magnetic Materials, Philadelphia, 18-21 November 1969
2663	Multiplet Structure in the Reflectance Spectrum of Europium Chalcogenides	J. O. Dimmock J. Hanus* J. Feinleib*	
2666	Magnetic and Optical Properties of the High and Low Pressure Forms of $CsCoF_3$	J. M. Longo J. A. Kafalas J. R. O'Connor J. B. Goodenough	
2668	Magnetic Ordering Effects in the Reflectance of EuS, EuSe and EuTe	W. J. Scouler J. Feinleib J. O. Dimmock T. B. Reed C. R. Pidgeon*	
2670	Localized Vs Band Magnetic Semiconductors	T. A. Kaplan R. A. Bari	
2679	Specific Heat of EuO	A. J. Henderson, Jr.* G. R. Brown* T. B. Reed H. Meyer*	

* Author not at Lincoln Laboratory.

† Titles of Meeting Speeches are listed for information only. No copies are available for distribution.

MS No.			
2703	Infrared Pumping of Microwave Lines of OH, H_2O, and H_2CO near IR Stars and Shockwaves	M. M. Litvak	131st Meeting of American Astronomical Society, New York, 8-11 December 1969
2723	Laser Raman Spectroscopy	A. Mooradian	Seminar, Stevens Institute of Technology, Hoboken, 3 December 1969
2723-A	Laser Raman Spectroscopy	A. Mooradian	Seminar, RCA, Princeton, 4 December 1969
2723-B	Laser Raman Spectroscopy	A. Mooradian	Seminar, University of Pennsylvania, 16 December 1969
2723-C	Raman Spectroscopy of Semiconductors and Its Applications	A. Mooradian	Topics in Quantum Electronics, University of California, Berkeley, 2 February 1970
2723-D	Laser Raman Spectroscopy	A. Mooradian	Seminar, University of Southern California, 3 February 1970
2723-E	Laser Raman Spectroscopy	A. Mooradian	Seminar, University of California, Irvine, 4 February 1970
2723-F	Laser Raman Spectroscopy	A. Mooradian	Seminar, California Institute of Technology, 3 February 1970
2731	Magneto-Optical Study of the Band Structure of BiSb Alloys	J. G. Mavroides	Seminar, Boston College, 3 December 1969
2734	OH and H_2O Masers in Infrared Stars	M. M. Litvak	Informal Seminar, Harvard College Observatory, 13 November 1969
2746	A New Variational Approach to the Question of Localized Vs Itinerant Electron Models	T. A. Kaplan	Physics Colloquium, University of Massachusetts, 12 December 1969
2748	Thermal Brillouin Scattering in Solids	A. S. Pine	Seminar, MIT, 21 November 1969
2762A	Anomalous Properties of the Vanadium Oxides	J. B. Goodenough	Annual Meeting of American Physical Society, Chicago, 26-28 January 1970
2778	N-P Junction Photodetector in InSb Fabricated by Proton Bombardment	A. G. Foyt W. T. Lindley J. P. Donnelly	IRIS Detector Specialty Group, Santa Barbara, 12-13 February 1970
2783	Two-Magnon Raman Scattering from Magnetic Insulators	S. R. Chinn	Physics Seminar, Bell Telephone Laboratories, Murray Hill, New Jersey, 15 January 1970

Reports

MS No.

2815	Remarks on the Mott Transition	T. A. Kaplan R. A. Bari	International Symposium on Atomic, Molecular, and Solid State Theory and Quantum Biology, Sanibel Island, Florida, 19-24 January 1970
2816	Spin Waves in the Alkali Metals	A. R. Wilson	Physics Seminar, Lowell Technological Institute, Lowell, Massachusetts, 14 January 1970
2824	Precision X-ray Scattering Measurements of Charge Density Distribution in Solids	P. M. Raccah	International Symposium of the Winter Institute, Sanibel Island, Florida, 23 January 1970

I. SOLID STATE DEVICE RESEARCH

A. LONG WAVELENGTH, SINGLE MODE, CW, $Pb_{1-x}Sn_xTe$ DIODE LASERS

Spectral measurements of the laser emission from a CW $Pb_{1-x}Sn_xTe$ diode laser with $x = 0.315$ show that the output is single mode with a peak emission at 31.8 μ. The measurements were made using a CsBr prism. A liquid-He-cooled In-doped Ge detector was used to measure the laser emission. The packaged diodes were mounted on a copper heat sink immersed in liquid He in a dewar equipped with an Irtran-6 inner window and a KRS-5 outer window. The single mode spectrum of a $Pb_{0.685}Sn_{0.315}Te$ diode laser, which at 31.8 μ is the longest semiconductor laser wavelength measured to date in the absence of a magnetic field, is shown in Fig. I-1. The threshold current density was 640 amp/cm^2, and single mode operation was possible for the lower current densities above threshold up to about 40°K. Single mode CW diode lasers have now been achieved at 12°K in the composition range from pure PbTe to $Pb_{1-x}Sn_xTe$ containing 31.5 percent SnTe. These devices can be tailored to emit at any wavelength between 6.5 and 31.8 μ.

A. R. Calawa
T. C. Harman

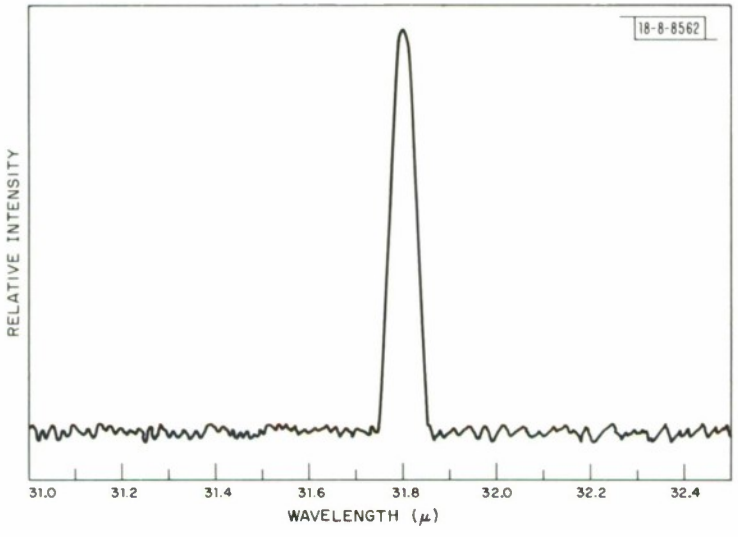

Fig. I-1. Emission spectrum of $Pb_{0.685}Sn_{0.315}Te$ diode laser at 1.8°K.

B. LOW CURRENT DENSITY THRESHOLD $Pb_{1-x}Sn_xTe$ DIODE LASERS

$Pb_{1-x}Sn_xTe$ lasers with unusually low current density thresholds have also been fabricated. Figure I-2 shows the relative infrared power emission at the 14-μ wavelength peak of a $Pb_{0.82}Sn_{0.18}Te$ diode laser with length $L = 5 \times 10^{-2}$ cm and width $W = 2.5 \times 10^{-2}$ cm at 12°K as a function of electrical current density. The threshold current density J_t of 20 amp/cm^2 is probably the lowest value ever obtained for a semiconductor laser. The result is consistent

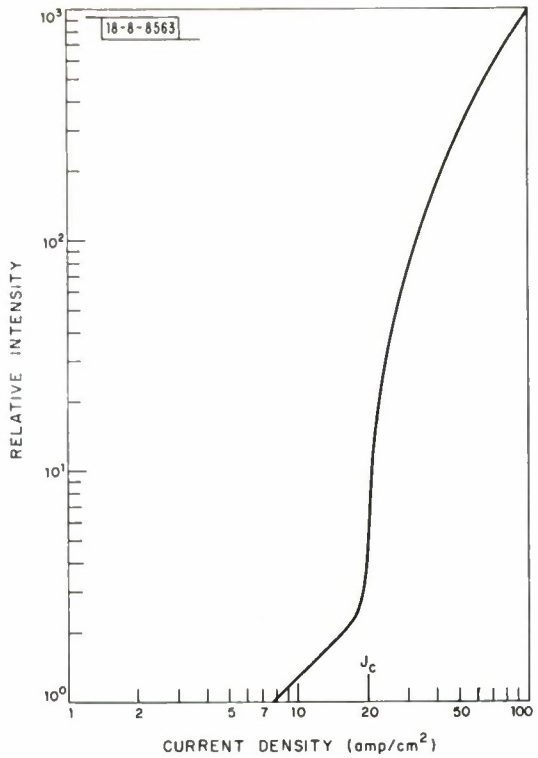

Fig. I-2. Relative emission intensity at 14 μ of a $Pb_{0.82}Sn_{0.18}Te$ diode laser at 12°K as a function of pulsed current density.

with theory, which indicates that J_t decreases as the energy gap E_G decreases, if all other factors remain the same. The appropriate theoretical expression is[1]

$$J_t = \frac{8\pi e n^2 E_G^2 d\Delta E}{c^2 h^3 \eta_i} \left(\alpha_T + \frac{1}{L} \ln \frac{1}{R}\right) \quad , \tag{1}$$

where n is the index of refraction, d is the width of the active region, ΔE is the spontaneous emission linewidth, α_T is the total loss per unit cavity length, L is the length of the Fabry-Perot or resonant cavity, R is the reflectivity, and η_i is the internal quantum efficiency. For the above $Pb_{0.82}Sn_{0.18}Te$ laser, the parameters have the following approximate values: n = 6, $d = 4 \times 10^{-3}$ cm, $E_G = 0.088$ eV, $\Delta E = 2 \times 10^{-3}$ eV, R = 0.5 and L = 0.05 cm. Using these values and assuming negligible losses ($\alpha_T = 0$) and unity internal quantum efficiency ($\eta_i = 1$), we obtain from Eq. (1) a calculated threshold current density J_t of 1.2 amp/cm^2. However, the internal loss factor α_T is not negligible. Preliminary measurements of the absorption coefficient at 12°K indicate a value of approximately 10 cm^{-1}. Using $\alpha_T = 10$ cm^{-1} and the experimental value for J_t, an internal quantum efficiency η_i of 0.15 is calculated. Possible significant contributions to α_T are those due to free carrier absorption, interband absorption and optical inhomogeneities. However, due to the Burstein shift for degenerate 5×10^{17}/cm^3 material, there is an increase in the minimum photon energy which can be absorbed by band-to-band transitions. Hence, the interband loss effect is probably relatively small. Both the free carrier absorption and scattering by optical inhomogeneities due to imperfections are probably significant loss mechanisms. The relatively low internal efficiency is probably due to nonradiative recombination processes.

Although a photoconductivity lifetime[2] of 10^{-6} has been measured on $6 \times 10^{15}/cm^3$ material, the lifetime is considerably lower for the $5 \times 10^{17}/cm^3$ doping level of the laser devices. If the diffusion length L is assumed to be d/2 or 20 μ, the carrier lifetime can be calculated from $\tau = eL^2/\mu_c kT$. For $\mu_e = 5 \times 10^5$ cm^2/V-sec and T = 4°K, this gives a value of $\tau = 2 \times 10^{-8}$ sec. This value of τ agrees within a factor of two with the lifetime obtained by extrapolating the measured photoconductive lifetime to the $5 \times 10^{17}/cm^3$ doping level.

T. C. Harman I. Melngailis
A. R. Calawa E. D. Hinkley

C. LOW TEMPERATURE ELECTRICAL PROPERTIES OF $Pb_{1-x}Sn_xTe$

The carrier type and carrier concentrations of Pb-Sn salt crystals are believed to be determined primarily by deviations from stoichiometry. Excess metal is the source of n-type carriers, whereas excess Te yields p-type material. By the use of proper annealing procedures, homogeneous crystals of both n- and p-type material can be achieved for $Pb_{1-x}Sn_xTe$ in the range x = 0 to x = 0.30. The Hall coefficient and electrical resistivity have been measured at various temperatures and for different carrier concentrations. Carrier concentrations and Hall mobilities determined for several crystals at 4°K are shown in Table I-1. It is seen that

TABLE I-1
SOME ELECTRICAL PROPERTIES OF ANNEALED $Pb_{1-x}Sn_xTe$ CRYSTALS AT 4°K

Crystal No.	x	Crystal Growth Technique	Hall Carrier Concentration at 4°K (cm^{-3})	Hall Carrier Mability at 4°K (cm^2/V-sec)
B	0.0	TGZM	5.6×10^{17} n	2.6×10^6
12C	0.13	Bridgman	3.0×10^{16} n	8.0×10^5
16-13E	0.17	Bridgman	1.8×10^{15} n	2.3×10^5
4-4	0.17	Bridgman	5.5×10^{16} n	5.0×10^5
8-34	0.20	Bridgman	2.6×10^{16} n	2.4×10^5
T-12	0.20	TGZM	2.5×10^{17} n	5.3×10^5
T-13	0.20	TGZM	4.1×10^{17} n	3.9×10^5
20B	0.20	Vapar	2.5×10^{17} n	4.6×10^5
20C	0.20	Vapar	1.8×10^{17} n	5.4×10^5
6B	0.30	Bridgman	2.2×10^{17} p	1.4×10^5

relatively high carrier mobilities are obtained, even though $Pb_{1-x}Sn_xTe$ is a pseudobinary alloy. Both Bridgman-grown and TGZM (temperature gradient zone melted) crystals contain some microscopic-sized metallic inclusions. There is no evidence for microscopic-sized metallic inclusions in bulk vapor grown material. As seen in Table 1-1, there is a trend toward lower carrier mobilities at higher Sn content. It is anticipated that significantly higher carrier mobilities can be achieved as the crystalline imperfection density is reduced.

T. C. Harman
A. E. Paladino

D. LASER EMISSION FROM $Pb_{1-x}Sn_xTe$ METAL-SEMICONDUCTOR DIODES

$Pb_{1-x}Sn_xTe$ diode laser emitters have been fabricated using evaporated metal contacts instead of conventional p-n junctions. Metals with small work functions (e.g. Pb, In, Zn, and Sn) produce a narrow degenerate inversion layer on the surface of p-type samples, as expected in the case of an ideal metal-semiconductor barrier which is not influenced by semiconductor surface states. If it is assumed that the role of surface states is negligible, the depth of the conduction band below the Fermi level at the surface is about 600 meV, the difference between the work function of Pb (4.0 eV) and the electron affinity of PbTe (4.6 eV). The resulting energy band diagram for the case of Pb on degenerate p-type PbTe is shown in Fig. 1-3. The three regions of the semiconductor include: (1) a 300-Å-wide inverted region near the metal-semiconductor interface, (2) a 600-Å depleted region, and (3) the p-type bulk extending to the right. The inverted region (1) acts as a source of injected electrons when the junctions are forward biased. The barriers obtained are strongly dependent on the work function of the evaporated metal, indicating a minimal role of surface states. Evidence that the surface regions are degenerately inverted by the presence of the metal comes from C-V data, and this picture

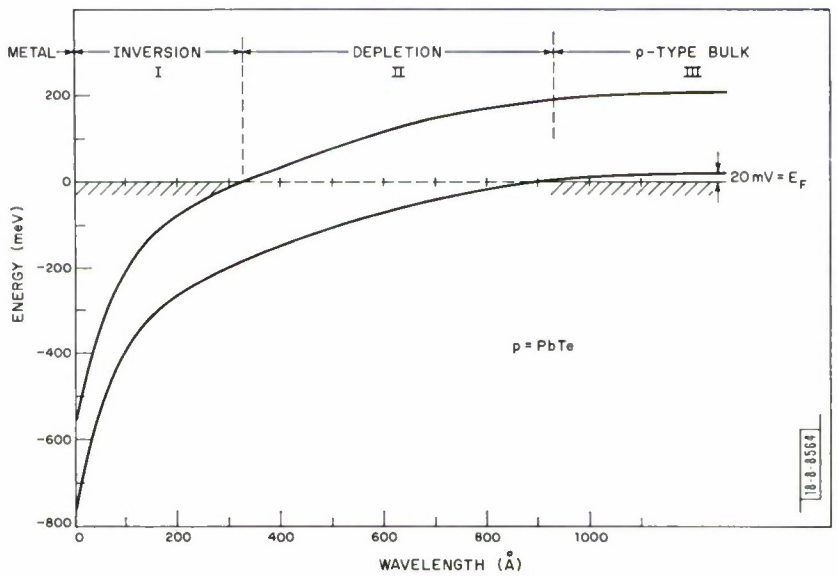

Fig. 1-3. Calculated barrier profile for lead evaporated on p-type PbTe ($p = 1 \times 10^{18}$ cm^{-3}, T = 0°K).

is confirmed by the low temperature laser emission reported here. Laser diodes were fabricated by evaporating approximately 1-μ-thick films of Pb, In, Zn, and Sn on fleshly etched surfaces of unannealed p-type material with $p = 3$ to 5×10^{18} cm^{-3}. During evaporation the samples were mounted on a liquid nitrogen cooled mask to avoid heating and consequential diffusion of the evaporated metal. Diodes on p-type PbTe with $p = 4 \times 10^{18}$ cm^{-3} showed zero-bias resistance-area products (RA) as high as 15 ohm-cm^2 at 77°, reducing in high forward bias to less than 2.5×10^{-6} ohm-cm^2. The zero-bias capacitance of these devices was approximately 6.8 μF/cm^2, indicating a depleted junction width of about 500 Å. Threshold current densities for laser emission compare favorably with the best p-n junction devices in PbTe with a minimum value observed here of 120 amp/cm^2. In addition to the laser emission obtained at 6.4 μ from PbTe, we have studied similar barriers on p-type $Pb_{0.80}Sn_{0.20}Te$ and have obtained laser emission at about 15 μ at 4.2°K. This work is continuing to determine the maximum laser wavelength that can be obtained from metal-semiconductor contacts on $Pb_{1-x}Sn_xTe$. Barriers have been produced on $Pb_{0.69}Sn_{0.31}Te$, although laser structures have not yet been fabricated.

K. W. Nill
J. N. Walpole
A. R. Calawa
T. C. Harman

E. DETERMINATION OF ACOUSTIC AMPLIFICATION COEFFICIENTS IN GaAs USING BRILLOUIN SCATTERING

Acoustic waves can be amplified in piezoelectric semiconductors by the application of electric fields that are high enough to cause the mobile charge carriers to drift at supersonic velocities. In high mobility materials, such as GaAs, the gain per unit length of the piezoelectrically-active acoustic waves is expected to be a linear function of the applied field. Hence, the amplitude of the waves propagating along the field direction grows exponentially until the waves reach the end of the sample or become of sufficient intensity to produce current saturation.[3]

We have begun measurements of the frequency dependence of the acoustoelectric amplification coefficients in n-GaAs using the Brillouin scattering apparatus shown schematically in Fig. I-4. A Xe arc lamp, filtered to provide a source in the range 9800 to 9920 Å, was focused onto the sample in an f/12 cone. The frequency of the acoustic wave producing scattering can

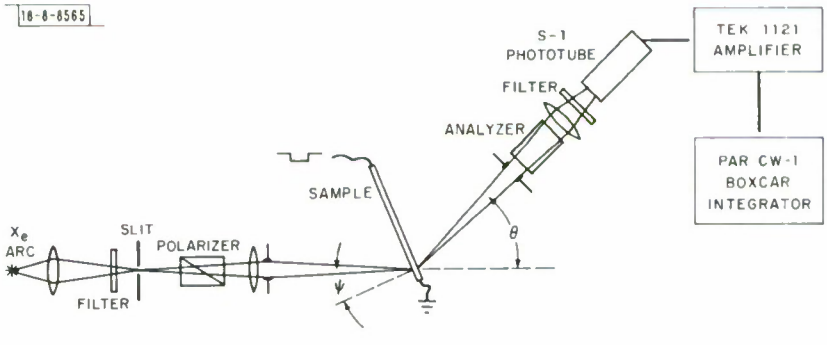

Fig. I-4. Schematic diagram of Brillouin scattering apparatus used to detect acoustoelectrically amplified shear waves in GaAs.

be determined directly from the angle of incidence ψ and the scattering angle Θ, which for the case $\Theta = 2\psi$ is given by

$$f = \frac{2nv_s}{\lambda_o} \sin \Theta/2 \quad ,$$

where n is the refractive index, λ_o is the wavelength in vacuum, and v_s is the sound velocity.

A broadband source of acoustic waves is provided simply by the Debye spectrum of the thermal background of lattice vibrations, a small portion of which is subsequently amplified by the application of the electric field. The f/9 acceptance cone of the detector optics limited our resolution of the acoustic spectrum to 0.3 GHz. The crossed polarizer/analyzer aided in isolating the shear wave scattering[4] from other possible scattering mechanisms.

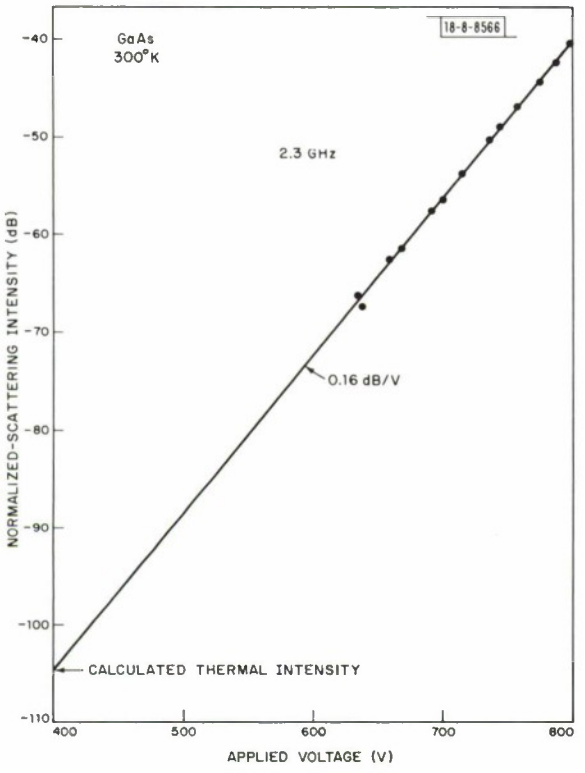

Fig. I-5. Scattering intensity (normalized to transmitted intensity) as a function of applied voltage.

Some preliminary results of measurements made at room temperature on 4 ohm-cm GaAs are shown in Fig. I-5. Here the scattering intensity at a position 24 mm from the cathode was sampled 7.4 μsec after the onset of 8-μsec voltage pulses. The scattering angle Θ was 40°, corresponding to a frequency of 2.3 GHz. As expected, the scattering intensity grows exponentially with applied voltage. Although similar growth occurred somewhat beyond 800 volts, domain formation[3] was observed at this point which greatly complicated the situation. The slope of the curve 0.16 dB/V is in good agreement with the thcoretical value of the acoustoelectric gain coefficient at 2.3 GHz.[5] By extrapolating the measured scattering intensity to that value calculated for a thermal distribution[4] we obtain the threshold voltage of 400 V. The corresponding threshold field of ~170 V/cm is in good agreement with that calculated from the theoretical gain coefficient and the measured nonelectronic attenuation coefficient.[6]

Since the frequency of the dctected acoustic wave can be changed by changing the scattering angle, we have an accurate and convenient way of measuring the frequency dependence of the gain. Modifications are being made which will extend these measurements to 77°K, wherc the amplification coefficient in high mobility epitaxial GaAs should be at least 20 times larger than observed here, with threshold fields as low as 3 V/cm.

D. L. Spears

F. TEMPERATURE AND CONCENTRATION DEPENDENCE OF ELECTRON MOBILITY IN HIGH-PURITY GaAs

The scattering mechanisms which determine the transport properties of GaAs were originally examined by Ehrenreich,[7] who showed that a combination of polar optical phonon and ionized impurity scattering yielded qualitative agreement with the temperature and impurity concentration dependence of the electron mobility for the purest bulk GaAs. Since then, vapor and liquid phase epitaxial techniques have been used to improve the quality of GaAs. Also, there are now sufficiently accurate additional experimental data (such as piezoelectric measurements) to examine the effects of other scattering mechanisms. Here we combine polar optical phonon, piezoelectric acoustic phonon, deformation potential acoustic phonon, ionized impurity and neutral impurity scattering in the relaxation time approximation to obtain results which are in good agreement with the temperature and concentration dependence of the electron mobility in high-purity GaAs.

For polar optical phonon scattering a universal relaxation time cannot be defined except at low and high temperatures, and it is neeessary to use a variational method to solve the Boltzmann equation[8] to determine the mobility of the electrons. However, following Ehrenreich[9] we use a relaxation time which is obtained from a variational calculation[10] and which gives the correct solutions to the Boltzmann equation at low and high temperatures. For GaAs this method of analysis fails completely from about 120° to 330°K (see Fig. 5 of Ref. 9) and this places an upper temperature limit of 115°K on our calculation. For the other scattering processes the relaxation time approximation is reasonably valid and we use the formulations of Meijer and Polder[11] for piezoelectric acoustic phonon scattering (with spherical averaging of the piezoelectric and elastic constants[12]), of Bardeen and Shockley[13] for deformation potential acoustic phonon scattering, of Brooks and Herring[14] for ionized impurity scattering, and of Erginsoy[15] for neutral impurity scattering. The electron mobility is then obtained by adding the reeiproeals of these individual relaxation times and numerically calculating an average relaxation time for a classical distribution of electrons.

In this calculation there are a number of parameters, most of which have or can be determined from other measurements. The shallow donor concentration N_D and the total aeceptor concentration N_A can be determined by fitting the experimental temperature variation of the Hall constant for each sample using the normal single donor statistics. Most of the other parameters are reasonably well known and the values we have used are listed in Table I-2. The least well-known parameter is probably the conduction band deformation potential with the only known experimental value being $|E_1| = 6.3\,eV$.[20] This value is therefore adjusted in the calculation to obtain agreement with the experimental mobility of the highest purity sample.

Figure I-6 shows the temperature variation of the experimental mobility measured at 5 kG and the calculated mobility for several samples. For the highest purity sample (Sample 1) the combined mobility is fairly sensitive to deformation potential scattering because of its strong energy dependence. That is, from 45° to 85°K a variation in the deformation potential of 10 percent produees a variation in the combined mobility of from 5 to 6 percent. The deformation potential was thus adjustcd to obtain agreement between the calculated and experimental mobility for Sample 1 in this temperature range. The best agreement was attained with $|E_1| = 7.0\,eV$.

TABLE I-2
PARAMETERS FROM LITERATURE

Electron Effective Mass	$m^*/m = 0.072$
Dielectric Constants	$\epsilon_o = 12.53$ (a) $\epsilon_\infty = 10.90$ (a)
Longitudinal Optical Phonon Temperature	$\theta_\ell = 423°K$ (b)
Piezoelectric Constant	$h_{14} = 1.41 \times 10^7$ V/cm (c)
Elastic Constants	$c_{11} = 1.221 \times 10^{12}$ dynes/cm^2 (d) $c_{12} = 0.566 \times 10^{12}$ dynes/cm^2 (d) $c_{44} = 0.599 \times 10^{12}$ dynes/cm^2 (d)

(a) Ref. 16
(b) Ref. 17
(c) Ref. 18
(d) Ref. 19

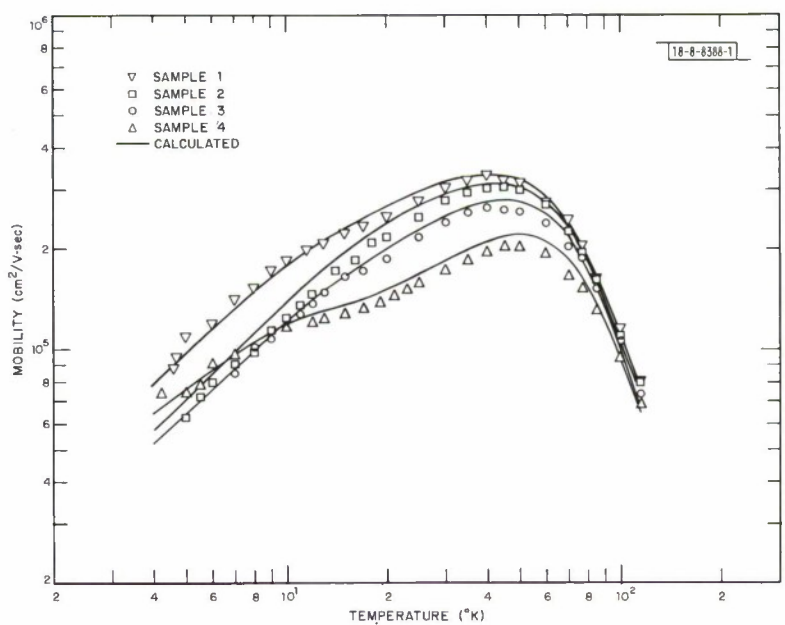

Fig. I-6. Temperature dependence of mobility for several samples showing calculated combined mobility curves and experimental points.

By using this value, the temperature variations of the combined mobility for the other samples (Samples 2, 3, 4) were calculated. As can be seen, there is good agreement between the calculated and experimental mobilities. The values of N_D and N_A for each sample as determined from the Hall constant analyses are listed in Table I-3. It should be emphasized that the agreement at low temperatures where ionized impurity scattering is dominant depends upon the accuracy of the values of N_D and N_A obtained from the Hall constant analyses.

TABLE I-3
PARAMETERS FROM HALL CONSTANT ANALYSES

Sample No.	N_D (cm^{-3})	N_D ($\times 10^{13} cm^{-3}$)	N_A/N_D
1	4.80×10^{13}	2.13	0.444
2	4.61×10^{13}	2.97	0.644
3	7.15×10^{13}	3.66	0.512
4	1.91×10^{14}	2.61	0.137

It is interesting to note that Sample 4 which is not as pure as Samples 2 and 3 has a higher experimental and calculated mobility at the lowest temperatures. As indicated in Table I-2, this sample is the least compensated sample ($N_A/N_D = 0.137$) and thus has fewer ionized impurities at low temperatures where the shallow donors are deionized. The contribution due to neutral impurity scattering is also more important for this sample.

Since the 77°K mobility is a commonly used figure of merit for GaAs, we have plotted experimental values in Fig. 1-7 as a function of total ionized impurity concentration ($N_D + N_A$) over the donor concentration range where sufficient donor deionization is observed to allow meaningful analyses of the temperature variation of the Hall constant. Also shown are values determined in a similar manner by Bolger, et al.[21] and Maruyama, et al.,[22] where the low-field mobility values of Maruyama, et al., were converted to the values that would be obtained at 5 kG. The curves shown were calculated using compensation ratios of $N_A/N_D = 0$ and $N_A/N_D = 0.5$, whereas our experimental values for this parameter varied from 0.14 to 0.65. The points which lie above the calculated zero compensation curve may be caused by uncertainties in determining N_D and N_A. In any case, there is reasonably good agreement between experimental and calculated values over this concentration range.

It can also be seen in Fig. 1-7 that the 77°K mobility is becoming increasingly less sensitive to ionized impurity scattering in the low concentration range and is approaching a lattice scattering limit. The calculation presented here yields a lattice limited mobility of 240,000 cm^2/V-sec at 77°K. The less accurate value obtained by simply combining the individual mobilities is 258,000 cm^2/V-sec. Since the experimental value at $N_D + N_A = 7 \times 10^{13} cm^{-3}$ is already

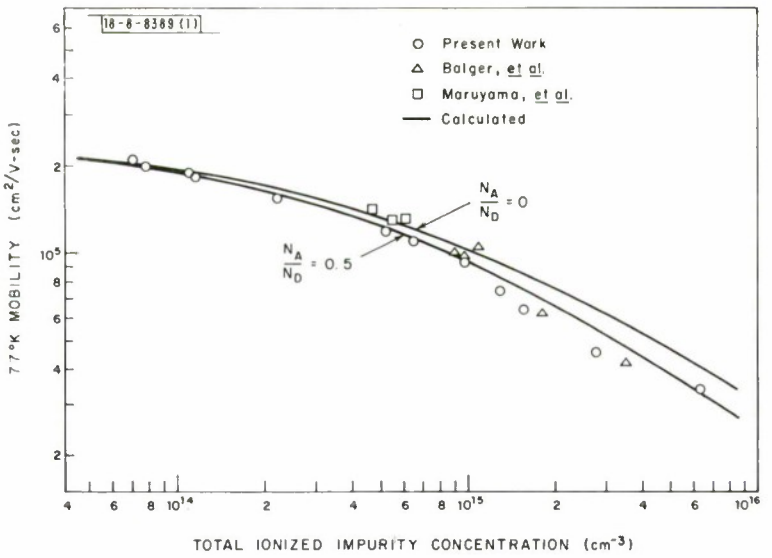

Fig. I-7. Cancentratian dependence of 77°K mability shawing curves calculated far twa campensatian ratios and experimental values.

210,000 cm^2/V-sec, at lower concentrations the 77°K mobility is no longer very useful as a figure of merit for GaAs.

C. M. Wolfe
G. E. Stillman
W. T. Lindley

G. PRESSURE DEPENDENCE OF ELECTRICAL RESISTIVITY OF EuO

The room temperature electrical resistivity of EuO is reported as a function of pressure up to 10 kbar. For the higher resistivity samples the pressure coefficient corresponds very closely to the observed shift of the optical absorption edge with pressure. Both the temperature and pressure dependence of the electrical resistivity are explained in terms of a model in which electrons are distributed between a temperature and pressure sensitive conduction band and a localized stationary trap level.

Two models have been proposed previously to explain the temperature and magnetic field dependence of the electrical resistivity in the Eu chalcogenides.[23-25] In both these models electrical conductivity at high temperature takes place through a thermally activated hopping process, and the large temperature and magnetic field dependence of the conductivity is ascribed to changes in electron mobility.

Recently, we have presented some evidence which indicates that the major part of the electrical resistivity variation near and below the Curie point in our undoped samples of EuO is due to changes in carrier density and not to mobility variations.[26,27] The observed dependence of the resistivity on temperature and magnetic field was found to be consistent with a model in which the conductivity occurs in an electron band which varies in energy in the same way as the optical absorption edge. In the model the carriers are thermally distributed between this conduction band and an electron trap state whose energy position is independent of temperature and magnetic field. The observed large changes in resistivity occur via a redistribution of electrons

between the eonduetion band and the trap as the eonduetion band moves. In order to eonfirm this model we have measured the pressure dependence of the electrical resistivity of EuO at room temperature. The results agree with our model of band eonduetivity and a stationary trapping level.

The resistivity versus pressure measurements were made at room temperature on a variety of EuO crystals. The results for three reprcsentative samplcs are shown in Fig. I-8. For the highest eonduetivity sample, the resistivity is independent of pressure. For the two highest resistivity samples the pressure coeffieient is given by

$$\frac{d \ln \rho}{dP} \simeq -0.20 \text{ kbar}^{-1} \quad .$$

If this variation is interpreted in terms of a pressure sensitive eleetrieal aetivation energy we obtain

$$kT \frac{d \ln \rho}{dP} \simeq -5.2 \text{ meV/kbar} \quad ,$$

which is very elose to the observed shift of the room temperature optieal absorption edge of -4.4 meV/kbar.[28]

The temperature dependenee of the resistivity for the same samples is shown in Fig. I-9. The two highest resistivity samples have a very high peak in the resistivity near T_c and an

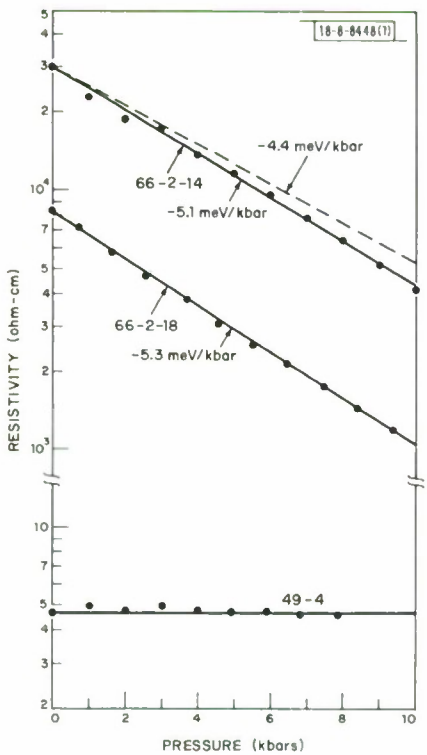

Fig. I-8. Resistivity versus pressure at raam temperature far three EuO samples.

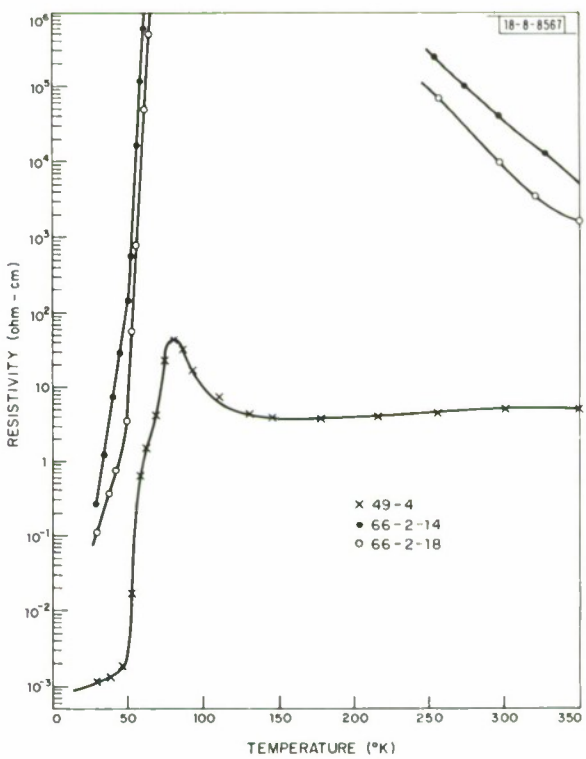

Fig. I-9. Resistivity versus temperature curves for three samples af Fig. I-8.

activation energy type behavior well above T_c with $\Delta E \simeq 0.28$ eV. The higher conductivity sample 49-4 shows a peak in the resistivity near T_c, but above the peak the resistivity remains relatively constant out to 350°K. All the curves show a large change in resistivity below T_c with a sharp break in slope near 50°K.

These results are consistent with a model which includes a conduction band whose energy varies with temperature and pressure as does the observed optical absorption edge, and a trap level whose energy is constant and equal to that of the conduction band minimum at 50°K and zero pressure. The proposed relative positions of the conduction band edge and trap level are shown in Fig. 1-10. The observed change in resistivity with temperature and pressure is consistent with a change in the number of conduction electrons brought about by the change in the relative positions of the conduction band and the trap level.

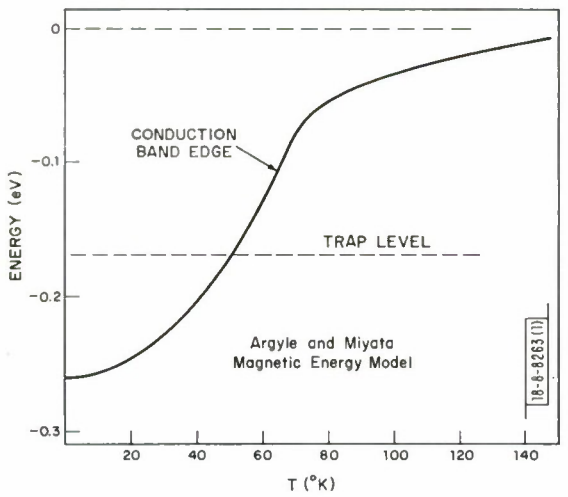

Fig. 1-10. Proposed model for conduction band and trap level as functions of temperature.

The resistivity variations with pressure shown in Fig. 1-8 strongly support the proposed model. In the high resistivity case where the electrons are supplied to the conduction band by thermal activation, the resistivity decreases as the band edge is lowered toward the trap level and more electrons are thermally excited into the band. The observed behavior of samples 49-4 is also expected from the model in consideration of the lack of temperature dependence of its resistivity.

M. R. Oliver J. O. Dimmock
J. A. Kafalas T. B. Reed

REFERENCES

1. M. I. Nathan, Proc. IEEE 54, 1276 (1966).
2. I. Melngailis and T. C. Harman, Appl. Phys. Letters 13, 180 (1968), DDC AD-688024.
3. D. L. Spears and R. Bray, Phys. Letters 29A, 670 (1969); D. L. Spears, IBM J. Res. Develop. 13, 499 (1969).
4. G. Benedek and K. Fritsch, Phys. Rev. 149, 647 (1966).
5. C. Jacoboni and E. W. Prohofsky, J. Appl. Phys. 40, 454 (1969).
6. D. L. Spears, Phys. Rev. (to be published).
7. H. Ehrenreich, Phys. Rev. 120, 1951 (1960).
8. D. J. Howarth and E. H. Condheimer, Proc. Roy. Soc. (London) A219), 53 (1953).
9. H. Ehrenreich, J. Appl. Phys. (Suppl.) 32, 2155 (1961).
10. _____, J. Phys. Chem. Solids 8, 130 (1959).
11. H. J. G. Meijer and D. Polder, Physica 19, 255 (1953).
12. J. D. Zook, Phys. Rev. 136, A869 (1964).
13. J. Bardeen and W. Shockley, Phys. Rev. 80, 72 (1950).
14. H. Brooks, Advan. Electron. Electron Phys. 7, 158 (1955).
15. C. Erginsoy, Phys. Rev. 79, 1913 (1950).
16. K. G. Hambleton, C. Hilsum and B. R. Holeman, Proc. Phys. Soc. (London) 77, 1147 (1961).
17. S. Iwasa, I. Balslev and E. Burstein, Physics of Semiconductors, Proceedings of the 7th International Conference Paris, 1964 (Academic Press, New York, 1964), p. 1077.
18. K. G. Hambleton, Phys. Letters 16, 241 (1965).
19. C. W. Garland and K. C. Park, J. Appl. Phys. 33, 759 (1962).
20. E. Haga and H. Kimura, J. Phys. Soc. Japan 19, 658 (1964).
21. D. E. Bolger, J. Franks, J. Gordon and J. Whitaker, Proceedings of the International Symposium on GaAs, Reading, 1966 (Institute of Physics and The Physical Society, London, 1967), p. 16.
22. M. Maruyama, S. Kikuchi and O. Mizuno, J. Electrochem. Soc. 116, 413 (1969).
23. S. von Molnar and S. Methfessel, J. Appl. Phys. 38, 959 (1967).
24. T. Kasuya and A. Yanase, Rev. Mod. Phys. 40, 684 (1968).
25. T. Penney, to be published in Proceedings 3rd International Conference on Photoconductivity, Stanford University, 1969.
26. C. E. Hurwitz, M. R. Oliver, J. O. Dimmock and T. B. Reed, Bull, Am. Phys. Soc. II, 14, 309 (1969).
27. M. R. Oliver, J. O. Dimmock and T. B. Reed, IBM J. Res. Develop. (to be published in May 1970).
28. P. Wachter, Solid State Commun. 7, 693 (1969).

II. MATERIALS RESEARCH

A. PHASE DIAGRAM OF PbTe-PbSe SYSTEM

Two substantially different phase diagrams have been published for the PbTe-PbSe pseudobinary system (Fig. II-1). Elagina and Abrikosov[1] reported a minimum in the liquidus and solidus curves at about 900°C and 0.18-mole fraction PbSe and a liquidus-solidus gap remaining less than 0.23-mole fraction. A more recent diagram by Grimes[2] shows no minimum in either curve and a gap attaining about 0.35-mole fraction.

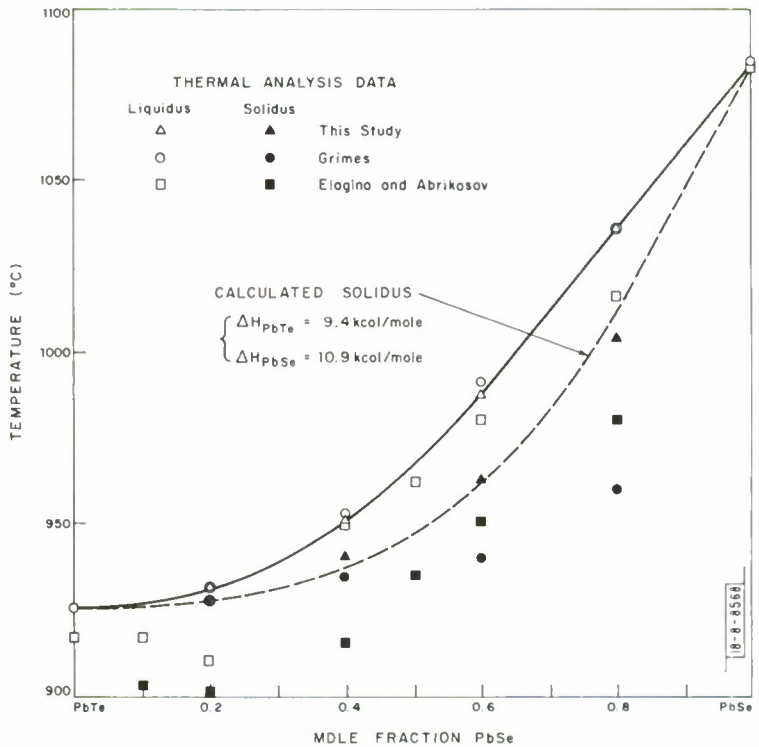

II-1. Phase diagram of PbTe-PbSe pseudobinary system.

The liquidus and solidus curves have now been redetermined by thermal analysis of cooling and heating eurves, respeetively, of homogenized liquid and solid solutions, using the same method as in previous studies of the CdTe-CdSe (Ref. 3) and CdTe-ZnTe (Ref. 4) systems.

The liquidus arrest temperatures observed in this study (Fig. II-1) are in exeellent agreement (±2°C) with the values reported by Grimes[2] and show a monotonic and sublinear variation with eomposition. However, the solidus arrest temperatures are systematieally higher than the values obtained in either previous investigation, and the liquidus-solidus gap remains less than 0.13-mole fraction.

The solidus curve shown in Fig. II-1 has been calculated from our liquidus data by using the ideal liquidus-solidus equation for binary systems (Ref. 5, Eq. II-6) and the values recommended

by Kulwicki[6] for the enthalpies of fusion of pure PbTe and PbSe. The calculated curve shows excellent agreement with our experimental solidus data. It is probable that the solidus temperatures reported by the previous investigators were low because their solid alloy samples were not completely homogenized.

J. M. Steininger

B. COMPOSITION STABILITY LIMITS OF $(Pb_{1-y}Sn_y)_{1-x}Te$ ALLOYS

To determine the composition stability limits of $(Pb_{1-y}Sn_y)_{1-x}Te_x$ alloys, samples were prepared from the spectroscopically pure elements for y = 1.0, 0.90, and 0.80 and for a number of values of x between 0.45 and 0.55. The synthesis, which was designed to yield equilibrated, powder samples, included a number of annealing steps. Each of these was carried out in a carbon-coated, evacuated, and scaled silica tube that had been previously outgassed for 16 hours at 1040°C and 10^{-7} Torr. Unless stated otherwise, each anneal was terminated by quenching in water. The synthesis steps were: (1) fusion of the weighed elements at 930°C, (2) (except for y = 1.0) furnace cooling to 800°C, annealing there for 16 hours, and furnace cooling to 400°C, (3) grinding the entire 20-gram sample in agate to 177 μm and annealing 120 hours at 750°C, (4) again grinding the entire sample to 177 μm and further grinding a 9-gram portion to 44 μm, (5) annealing the 44 μm powder in 3-gram batches for 120 hours either at 400°C or for Te-rich samples (which were found to sinter at 400°C) at 350°C. A final step for compositions found to lie within the stability field consisted of reduction for 1 hour between 550° and 600°C with H_2 at 600 Torrs.

The x-ray pattern for each powder was taken at 25.0 ± 0.3°C with 40 kV, 40 mA, CuK_α radiation using a Philips diffractometer with a 1° divergence slit and a curved LiF monochromator in the diffracted beam. A scanning speed of 1/4°/min in 2Θ and a chart speed of 30 in./hour allowed the value of 2Θ to be read with a precision of ±0.005°. A 2Θ-correction curve was established with Si (a_o = 5.4301 Å) and 99.99% W-powder (a_o = 3.1650 Å). Zinc-saturated ZnTe (a_o = 6.1026 Å) was used as a secondary standard. The lattice parameter (a_o) of the cubic $(Pb_{1-y}Sn_y)_{1-x}Te_x$ phase was calculated from the corrected positions of 14 diffraction lines by a computer minimization of the function $\sigma = \left\{ \sum_{L=1}^{14} (2\Theta_{i,obs} - 2\Theta_{i,cal})^2/14 \right\}^{1/2}$. Typically σ had a value of 0.01°, which corresponds to a standard deviation in a_o of $2(10^{-4})$ Å. The observed line half-widths, which were in the range of 0.10° to 0.17° in 2Θ, were essentially determined by the instrumental limits.

When a_o is plotted against the overall atom fraction of Te for y = 1.0 (SnTe), a_o is constant for compositions in the Sn-rich two-phase field, decreases linearly and rapidly as x increases within the stability field, and becomes constant at the Te-rich limit. The behavior for the ternary alloys, y = 0.90 and 0.80, is qualitatively similar except that a_o changes slowly in the two-phase regions. (This slow change shows the liquid-solid tie lines in the ternary system are not lines of constant y.) The variation of a_o (in angstroms) within the stability field is given by $a_o = 6.3279 - 3.53(x - 1/2)$ for y = 1.0, $a_o = 6.3400 - 2.69(x - 1/2)$ for y = 0.90, and $a_o = 6.3540 - 2.75(x - 1/2)$ for y = 0.80. The metal-rich stability limit at 400°C is x = 0.5000 for all three values of y. The Te-rich stability limit at 350°C is x = 0.5070 for y = 1.0, 0.5058 for y = 0.80 and 0.5037 for y = 0.90. The estimated uncertainty in the stability limits is $\pm 2(10^{-4})$ in x.

The values of a_o for x = 1/2 are within 0.001 Å of those obtained by Bis and Dixon[7] on single crystal thin films with hole concentrations in the $3\text{-}7(10^{19})$ cm^{-3} range. The values of a_o for compositions outside the homogeneity range are generally within 0.001 Å of those reported by Strauss.[8]

For compositions within the stability field of the ternary alloy, the values of a_o were observed to be $2(10^{-3})$ to $3(10^{-3})$ Å smaller before H_2-reduction than after. No change in a_o is observed when either H_2-reduced or unreduced powder is exposed to air at room temperature for several weeks. No change in a_o is observed when a H_2-reduced powder is sealed off under vacuum and annealed for 120 hours at 400°C (or 750°C for x = 1/2, y = 0.80), if the powder is not exposed to air between reduction and seal-off. However, a decrease in a_o is observed if H_2-reduced powder is exposed to air at room temperature for even a few minutes, then sealed off under vacuum and annealed for only 16 hours at 350°C. These observations can be explained in the following manner. When a fine, oxygen-free telluride powder is exposed to air at room temperature, there is a rapid reaction with oxygen. This reaction is confined to a relatively thin surface layer of each particle and causes no change in the measured a_o. When the powder is heated, the oxygen reacts with metal throughout the particle, causing an increase of about $5(10^{-4})$ in x and consequent decrease in a_o. Reduction with H_2 restores the metal to the telluride phase, causing a_o to increase to its original value.

R. F. Brebrick

C. PRESSURE-INDUCED PYROCHLORE TO PEROVSKITE TRANSFORMATIONS IN $Sr_{1-x}Pb_xRuO_3$ SYSTEM

The compound $SrRuO_3$ has been studied in some detail[9,10,11] and shown to be metallic and ferromagnetic with an orthorhombic perovskite structure. In an attempt to study the lead analog of this perovskite ($PbRuO_3$), PbO and RuO_2 (1:1) were reacted in air at 900°C. The product was an oxygen deficient pyrochlore $Pb_2Ru_2O_{7-x}$ with x in the range between 0.6 and 1.0 (Ref. 12). Physical measurements showed this material to be metallic and Pauli paramagnetic. Other oxygen-deficient pyrochlores are known in which x reaches one, as in $PbTcO_3$ (Ref. 13) and $AgSbO_3$ (Ref. 14), the defect pyrochlore structure thus becoming competitive with the perovskite structure.

The cubic pyrochlore structure, with general formula $A_2B_2O_7$, has the large A cation in eightfold coordination (nearly an hexagonal bipyramid) and the smaller B cation in octahedral coordination. There are two types of tetrahedral positions for the anions: six have two A and two B near neighbors and one has only A-cation near neighbors. The structures of $Pb_2Tc_2O_6$ (Ref. 13), $Pb_2Ru_2O_{7-x}$, $Pb_2Ir_2O_{7-x}$, and $Pb_2Re_2O_6$ (Ref. 12) are thought to be derived from that of pyrochlore by selective removal of the anions having only A-cation near neighbors. At the limiting value of x = 1, the A cation would have only sixfold coordination.

In the perovskite structure (ABO_3) the B cation has octahedral coordination while the larger A cation has twelvefold coordination. For the composition ABO_3, the perovskite is generally favored at high pressures, as illustrated by $YMnO_3$ (Ref. 15), $CdTiO_3$ (Ref. 16) and $SrIrO_3$ (Ref. 17). Recently a number of defect pyrochlores (x = 1), including $BiYO_3$ and $BiSeO_3$ (Ref. 18,19), have been transformed to perovskites at high pressure. In preliminary work[12] we have shown that the perovskite structure of $PbRuO_3$ can be stabilized at high pressure and temperature (90 kbar,

1400°C). We have now investigated the complete composition range for the system $Sr_{1-x}Pb_xRuO_3$ at high pressure and present a pressure-composition phase diagram at 1400°C.

Ambient-pressure materials were prepared at 1000°C by the solid state reaction of $SrCO_3$, PbO and RuO_2 in stoichiometric proportions. Frequent regrindings were necessary to assure attainment of equilibrium. All high-pressure specimens were made using $SrRuO_3$, PbO and RuO_2, since $SrCO_3$ is unreactive at high pressure and the use of SrO is inconvenient due to its rapid uptake of CO_2 and H_2O during sample preparation. Stoichiometric amounts of the reactants were ground with an agate mortar and pestle and loaded into capsules made of platinum tubing (0.01 in. thick × 0.5 in. long × 0.15 in. diameter) and fitted with 0.1-in. thick platinum end plugs. The reactions were performed in a high-pressure belt apparatus[20] capable of developing pressures to 90 kbar. Pressure calibration of the apparatus was accomplished by observing the resistance discontinuities at the transition points of Bi, Tl, and Ba as reported by Kennedy and LaMori.[21] A tubular graphite heater was used in the pressure cell. In a typical run, the specimen was first subjected to the desired pressure; then the temperature was raised rapidly and held for 15 minutes. The specimen was quenched to room temperature before the pressure was released.

Phase and structural analysis of powdered samples was carried out with a Norelco vertical x-ray diffractometer using monochromated (LiF crystal) CuK_α radiation. The concentrations of the components in a two-phase region were estimated from the relative intensities of their diffraction patterns. Cell dimensions of the products were determined to ±0.003 Å by refinement of 2Θ values obtained from a slow diffractometer scan (1/4°/min).

The results of phase studies in the $Sr_{1-x}Pb_xRuO_3$ system as a function of pressure at 1400°C are summarized in Fig. II-2. Lattice parameters a, b, and c of the quenched phases at intervals of x = 0.2 are given in Table II-1. The c-axis changes very little and remains constant above $x \approx 0.5$. Also $c/\sqrt{2}$ gradually changes from greater than a to less than a. It is assumed that for $x > 0.5$, cooperative Pb-O interactions become significant and introduce distortions different from those found in the orthorhombic perovskite $SrRuO_3$. Table II-2 lists the observed d-values and intensities for a powder diffraction pattern of the perovskite form of $PbRuO_3$.

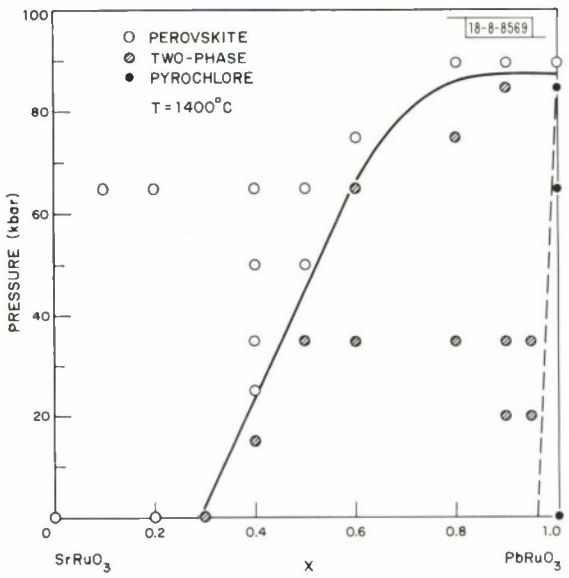

II-2. Pressure-composition phase diagram for $Sr_{1-x}Pb_xRuO_3$ system at 1400°C.

The solubility of Pb in the perovskite system $Sr_{1-x}Pb_xRuO_3$ extends to approximately x = 0.3 at atmospheric pressure and increases linearly with pressure to about x = 0.6 at 70 kbar. The pressure needed to stabilize the perovskite structure rapidly levels off above x = 0.7, and only about 90 kbar is required for the end member perovskite $PbRuO_3$. The formation pressure for the perovskite phase was found to increase as the temperature was decreased. The solubility of

TABLE II-1

CRYSTALLOGRAPHIC DATA FOR $Sr_{1-x}Pb_xRuO_3$ (Perovskite Structure)

x	a (Å)	b (Å)	c (Å)	Volume ($Å^3$)	$c/\sqrt{2}$ (Å)
0 ($SrRuO_3$)	5.530	5.570	7.847	241.7	5.550
0.2	5.537	5.579	7.851	242.6	5.552
0.4	5.545	5.588	7.856	243.4	5.556
0.6	5.549	5.596	7.864	244.2	5.562
0.8	5.555	5.603	7.863	244.7	5.561
1 ($PbRuO_3$)	5.562	5.610	7.862	245.3	5.560

TABLE II-2

X-RAY DATA FOR HIGH PRESSURE $PbRuO_3$ (Perovskite Structure)

hkl	d_{obs}	I_{obs}	hkl	d_{obs}	I_{obs}
110,002	3.948	M	242	1.193	VW
111	3.531	VW	422,026,206	1.187	VW
200,112,020	2.782	VS	044	1.141	W
021	2.620	VW	404	1.135	W
211,103	2.506	VW	226	1.091	VW
022	2.279	W	152,224	1.060	M
202	2.266	W	136	1.056	M
113	2.174	VW	424,512,316	1.053	M
220,004	2.061	S	440	0.988	VW
023,221	1.992	VW	008,441	0.982	VW
130	1.773	VW	060	0.935	VW
222,310,114	1.766	W	352	0.932	W
132	1.616	M	532,336,061	0.928	M
024,204,312	1.605	S	028,600,208	0.926	W
313,115	1.462	VW	260	0.886	VW
040	1.403	W	444	0.882	VW
224,400	1.393	M	261,063	0.880	M
330,134	1.316	W	620,228		
314,402,006	1.310	W	064	0.844	W
240	1.253	W	156	0.842	M
332	1.248	M	516,604	0.838	W
116,420	1.244	M	247,445	0.836	VW

a = 5.562 Å b = 5.610 Å c = 7.862 Å

Sr in the pyrochlore phase at all pressures was below our limits of detection. This very limited solubility of the basic Sr^{2+} ion is consistent with the known chemistry of the pyrochlore structure, which is stabilized by acidic and highly polarizable A cations such as Ag^{1+}, Pb^{2+} and Bi^{3+}.

The formation of the perovskite phase of $PbRuO_3$ could be accomplished by the pressure treatment of either a $PbO:RuO_2$ mixture or the oxygen-deficient pyrochlore phase prepared at atmospheric pressure. The pressure and temperature of perovskite formation were essentially the same for both routes. It is assumed that any excess oxygen of the deficient pyrochlore is lost from the pressure cell on transformation to the perovskite phase.

The x-ray density of the quenched, high-pressure perovskite phase of $PbRuO_3$ is about 10 percent greater than that of the pyrochlore. The stability of the perovskite to retransformation at atmospheric pressure is much lower than for other ruthenium perovskite and perovskite-related compounds.[22] Specimens treated at 450°C in flowing N_2 gas showed very slow retransformation (one-third conversion in 15 hours) while treatment at 500°C for 3 hours gives complete retransformation to the pyrochlore, presumably with $x = 1.0$ in this case. In contrast $Sr_{0.7}Ba_{0.3}RuO_3$, a high-pressure perovskite, shows no sign of transformation up to 1100°C (Ref. 22).

Preliminary magnetic measurements on the system $Sr_{1-x}Pb_xRuO_3$ show that the Curie temperature falls more and more rapidly with increasing x from 160°K for $x = 0$ to near 0°K for $x = 0.5$. The perovskite $PbRuO_3$ exhibits a magnetic behavior similar to the perovskite $CaRuO_3$ (Ref. 10).

J. A. Kafalas
J. M. Longo
D. A. Batson

REFERENCES

1. E. I. Elagina and N. Kh. Abrikosov, Dokl. AN SSSR 111, 353 (1958).
2. E. E. Grimes, Trans. Met. Soc. AIME 233, 1442 (1965).
3. Solid State Research Report, Lincoln Laboratory, M.I.T. (1969:3), p. 21, DDC AD-696620.
4. Solid State Research Report, Lincoln Laboratory, M.I.T. (1969:4), pp. 13-16, DDC AD-701022.
5. Solid State Research Report, Lincoln Laboratory, M.I.T. (1969:1), p. 33, DDC AD-687100.
6. B. M. Kulwicki, "The Phase Equilibria of Some Compound Semiconductors by DTA Calorimetry," Ph. D. Thesis, University of Michigan (1963).
7. R. F. Bis and J.R. Dixon, J. Appl. Phys. 40, 1918 (1969).
8. A. J. Strauss, Bull. Am. Phys. Soc. 14, 310 (1969); Solid State Research Report, Lincoln Laboratory, M.I.T. (1969:2), p. 9, DDC AD-690997.
9. A. Callaghan, C.W. Moeller and R. Ward, Inorg. Chem. 5, 1572 (1966).
10. J. M. Longo, P. M. Raccah and J. B. Goodenough, J. Appl. Phys. 39, 1327 (1968).
11. Y. Noro and S. Miyahara, J. Phys. Soc. Japan 27, 518 (1969).
12. J. M. Longo, P. M. Raccah and J. B. Goodenough, Mat. Res. Bull. 4, 191 (1969).
13. O. Muller, W. B. White and R. Roy, J. Inorg. Nucl. Chem. 26, 2075 (1964).
14. A. W. Sleight, Mat. Res. Bull. 4, 377 (1969).
15. A. Waintail and J. Chenavas, Compt. Rend. Acad. Sci. Paris 264, 168 (1967); Mat. Res. Bull. 2, 819 (1967).
16. J. Liebertz and C. J. M. Rooymans, Z. Phys. Chem. 44, 242 (1965).
17. J. M. Longo and J. A. Kafalas, 156th American Chemical Society Meeting, September 1968, INOR-4.
18. Yu. Ya. Tomashpolskii, Ye. U. Zubova, K. P. Burdina and Yu. N. Venevtsev, Izv. AN SSSR, Neorgan. Mater. 3, 2132 (1967); Inorg. Mater. (English Translation) 3, 1861 (1967).
19. Yu. Ya. Tomashpolskii, Ye. U. Zubova, K. P. Burdina and Yu. N. Venevtsev, Kristallografiya 13, 987 (1968); Soviet-Phys.-Cryst. (English Translation) 13, 859 (1969).
20. H. T. Hall, Rev. Sci. Instr. 31, 125 (1960).
21. G. C. Kennedy and P. N. LaMori, Progress in Very High Pressure Research, F. Bundy, W. Hibbard and H. Strong, Eds. (Wiley, New York, 1961), pp. 304-314.
22. J. M. Longo and J. A. Kafalas, Mat. Res. Bull. 3, 687 (1968).

III. PHYSICS OF SOLIDS

A. ELECTRONIC BAND STRUCTURE

1. Optical Reflectance Spectrum of Single Crystal Ti_2O_3

The optical reflectance spectrum of polished single-crystal Ti_2O_3 has been measured at 300°K in the photon energy range 0.1 to 11.0 eV. This material which is semiconducting at room temperature is of interest because it undergoes a semiconductor-to-metal transition around 400°K. In an attempt to understand the band structure, we are measuring the optical properties as a function of temperature. To date we have measured only the room temperature reflectance spectrum, but measurements at higher temperatures are in progress. The reflectance at 300°K is characterized by a slightly structured peak around 1 eV and three other peaks at 2.8, 5.3 and 8.2 eV, as shown in Fig. III-1.

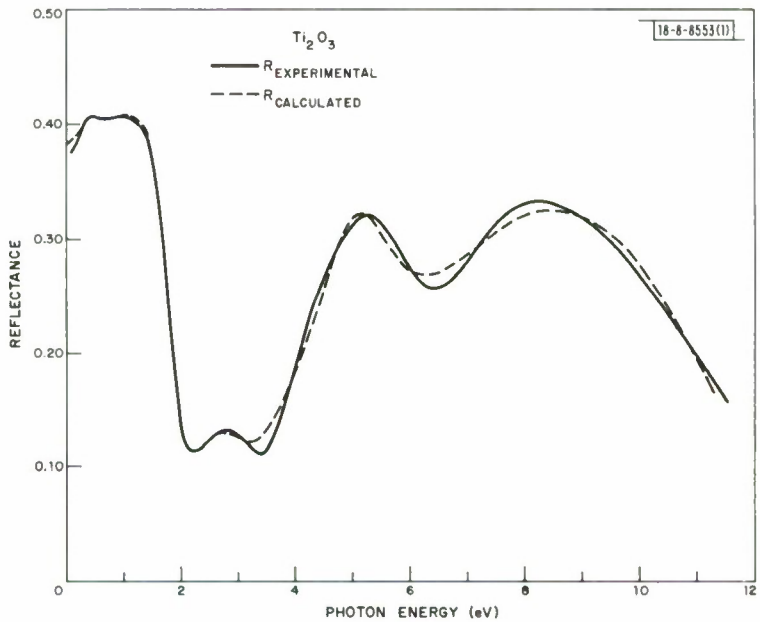

Fig. III-1. Experimental and calculated reflectance of Ti_2O_3.

In addition to the usual Kramers-Kronig analysis to yield the dielectric constant components ϵ_1 and ϵ_2, we have also performed a least-squares fit of the reflectance assuming that ϵ_1 and ϵ_2 can be represented by a sum of Lorentzian-type oscillators of the form

$$\epsilon_1 = 1 + \sum_i \frac{A_i \omega_p^2 (\omega_i^2 - \omega^2)}{(\omega_i^2 - \omega^2)^2 + \omega^2 \gamma_i^2} \quad , \qquad \epsilon_2 = \sum_i \frac{A_i \omega_p^2 \omega \gamma_i}{(\omega_i^2 - \omega^2)^2 + \omega^2 \gamma_i^2} \quad ,$$

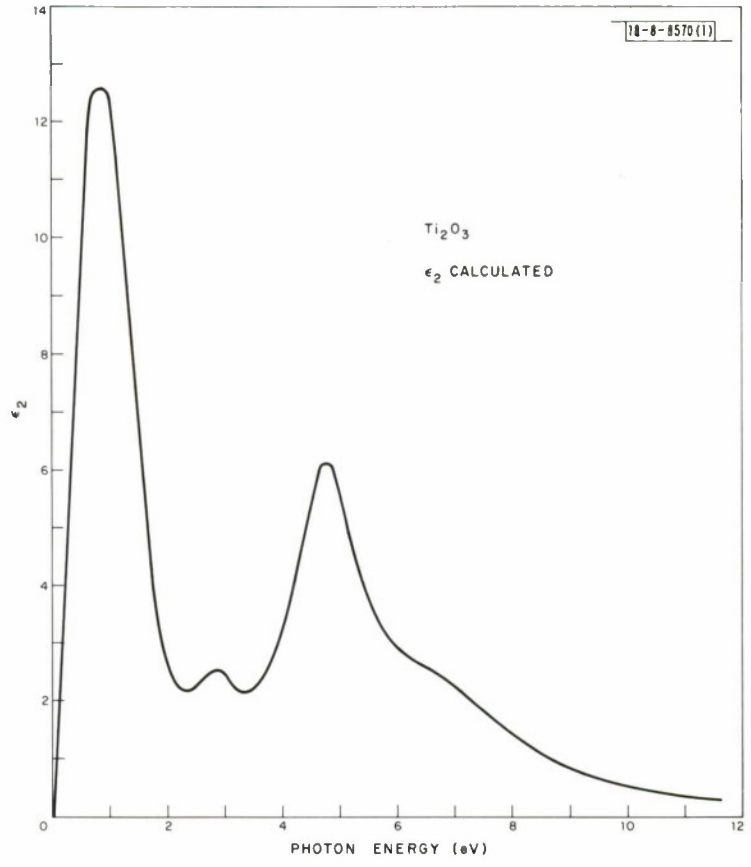

Fig. III-2. Imaginary component of dielectric constant, ϵ_2, calculated from least-squares fit.

where A_i is the oscillator strength, and the other symbols have their usual meaning. A good fit was obtained with the experimental reflectance using six oscillators: three centered around 1 eV at 0.7, 1.0 and 1.4 eV and the others, at 2.9, 4.8 and 6.8 eV, respectively. Figure III-1 gives the reflectance calculated from the computed ϵ_1 and ϵ_2 while Fig. III-2 shows ϵ_2. The weak oscillator strengths obtained for the four lowest energy oscillators imply that these transitions are predominantly between d-bands. When the measurements at higher temperatures have been made, a fuller interpretation of the results will be possible.

P. M. Raccah
W. J. Scouler

2. Quasi-Particle Approach to the Optical Properties of Simple Metals

Because of the strong electron-electron interaction in metals, many-body contributions in the optical absorption have to be carefully examined. The purpose of this work is to study the optical properties of simple metals when many-body effects are included.

The optical conductivity of a simple metal can be expressed in terms of the many-electron states in the absence of the perturbing electromagnetic wave according to the Kubo formula.[1] We find that the many-electron states in a simple metal can be expressed in terms of Bloch-like

quasi-particle-hole-pair excited states. The optical conductivity obtained from these states can be described in terms of an optical mass and the interband optical absorption in a form analogous to that found in the independent particle model.[2] Many-body effects that are included in the effective pseudopotential and quasi-particle energies can be interpreted in terms of the dynamical screening of the electron-ion interaction[3] and the possibility of collective excitations.[4] Numerical estimates in Na and Al indicate that moderate enhancements of the optical absorption, which is proportional to the square of the effective pseudopotential, are present due to many-body effects. However, these many-body enhancements of the effective pseudopotential are also present in the energy band structures and thus cannot be determined experimentally. Electron-electron collision contributions are neglected in the general discussion.

Our study indicates that the optical properties of simple metals can be calculated without an accurate determination of the many-body contribution provided the energy band structure is known from measurements of phenomena such as the dHvA effect. Indeed our investigation constitutes a justification of the validity of the commonly used independent particle model in optical calculations when many-body effects are taken into account.

C. Y. Young

3. Theory of Surface Plasmon Excitation in Electron Tunneling, Low Energy Electron Diffraction and Photoemission

The theory of inelastic electron tunneling due to surface plasmon (SP) excitation has been reviewed. It has been shown that electron tunneling is a powerful spectroscopic tool for investigating the SP excitation spectrum. Existing tools for the study of SP, such as electron energy loss experiments, optical excitation and transition radiation all suffer from the complexity of the excitation mechanism. The various accompanying effects that can occur in the solid make the extraction of the SP parameters rather difficult. In contradistinction to these tools, electron tunneling excitation of SP involves a much simpler mechanism. Useful information about SP, such as its dispersion and damping can be easily extracted from the tunneling data. The results obtained clearly indicate that electron tunneling can be developed to be a very sensitive probe for SP excitations. We have recently extended the treatment of inelastic scattering of electrons by SP to low energy electron diffraction (LEED) and photoemission. The theory is developed by using the two-potential formula of scattering theory. Results of the calculations give quantitative support to the interpretations of some prominent inelastic effects as due to SP excitation for recent experiments in LEED and photoemission carried out elsewhere.

K. L. Ngai
E. N. Economou*
M. H. Cohen*

4. Electrical Conductivity in the Hubbard Model

The following is an abstract submitted for the March Meeting of the American Physical Society to be held in Dallas, 23-26 March 1970.

---

* James Franck Institute, University of Chicago.

"The electrical conductivity for a system of electrons described by the single band Hubbard Hamiltonian is studied. An expression for the electrical conductivity that is applicable in the narrow band regime, i. e., bandwidth, Δ, much smaller than intra-atomic Coulomb repulsion, U, is derived. It is shown that the conductivity vanishes at T = 0 to first order in Δ/U for one electron per atomic site. For the non-half-filled band case, the degeneracy of the (atomic limit) ground state wave function plays a crucial role in yielding a non-zero value for the conductivity. The theory is applied to analyze the experimental data in Li-doped NiO. It is demonstrated how, as a consequence of this theory, the contribution to the conductivity from the narrow $3d^8$ band is suppressed in the total conductivity."

D. Adler*
R. A. Bari
R. V. Lange†

B. MAGNETISM

1. Remarks on Insulator-Metal Transition

In a series of papers beginning with the work of des Cloizeaux,[5] the most recent one being that of Langer, Plischke and Mattis,[6] the thermal Hartree-Fock approximation (THFA) has been applied to the Hubbard Hamiltonian. The phase transition that occurs at temperature T_M has been interpreted[5, 6] as a transition from a magnetically disordered insulator to a nonmagnetic metal (with increasing T).

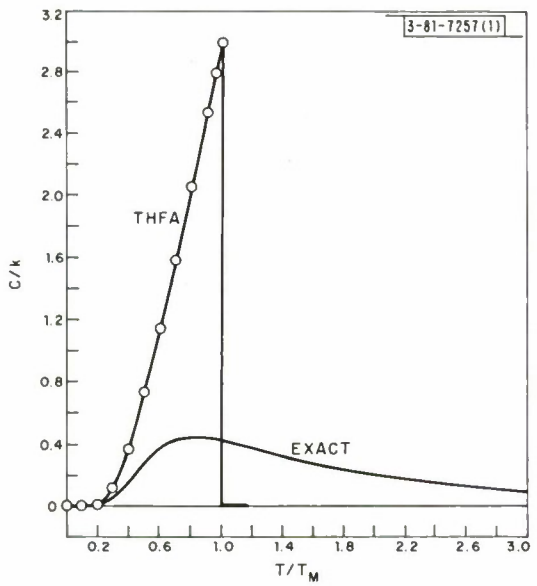

Fig. III-3. Specific heat is plotted os o function of temperature.

* Department of Electrical Engineering, M.I.T.
† Department of Physics, Brandeis University.

We make the following remarks:

(a) The interpretation of the transition at T_M as such a transition is incorrect, since, as calculated in the THFA by these authors, there is magnetic order (antiferromagnetic) for all T below T_M. In fact, this theory is essentially Slater's band antiferromagnetism which was criticized by Mott as being inadequate for a large class of materials (e.g., NiO), where the Néel temperature does not coincide with an insulator-metal transition!

(b) A transition at $T \approx T_M$ probably does not occur in the exact treatment of the Hubbard model, for small ratio Δ/U of bandwidth to intra-atomic Coulomb repulsion. Our reasons for making this statement are as follows. In the atomic limit ($\Delta/U \to 0$) the exact behavior (which is readily calculable) exhibits no phase transition. In particular, the specific heat in the THFA shows a very pronounced discontinuity at $T_M(=U/4k)$, and is thus an extremely poor approximation to the exact specific heat, which is a very smooth function of T (see Fig. III-3). Hence there is no reason for believing the suggestion, due to the THFA, that there is a transition at $T \approx T_M$, for Δ/U small but non-zero. Furthermore, the thermal single-determinant approximation,[7] a variational generalization of the THFA which, however, gives the exact behavior for $\Delta/U = 0$ (and for $U = 0$), yields no high-temperature transition for small Δ/U.

T. A. Kaplan
R. A. Bari

2. Theory of Spin Configurations in Cr_5S_6

Although there is some question regarding the validity of applying the Heisenberg Hamiltonian to a high-conductivity material such as Cr_5S_6, it has proved a fruitful approach in other materials with metallic conductivity, and it is of interest to establish its ability to account for the observed magnetic properties of Cr_5S_6. The classical Heisenberg energy is given by

$$E = \Sigma_{n\nu,m\mu} \bar{J}_{n\nu,m\mu} \vec{S}_{n\nu} \cdot \vec{S}_{m\mu} \qquad (1)$$

where $\vec{S}_{n\nu}$ and $\vec{S}_{m\mu}$ are unit vectors along the direction of spin quantization, n and m run over the unit cells in the sample, ν and μ run over the ten magnetic sites within a unit cell (shown in Fig. III-4), and the $\bar{J}_{n\nu,m\mu}$ are the usual exchange constants multiplied by the spin magnitudes. There are nine distinct nearest-neighbor (nn) interactions to be considered, typified by: $\bar{J}_1 \equiv \bar{J}_{n1,n2}$, $\bar{J}_{1'} \equiv \bar{J}_{n6,n7}$, $\bar{J}_2 \equiv \bar{J}_{n1,n5}$, $\bar{J}_{2'} \equiv \bar{J}_{n4,n7}$, $\bar{J}_{2''} \equiv \bar{J}_{n5,n8}$, $\bar{J}_3 \equiv \bar{J}_{n3,n7}$, $\bar{J}_{3'} \equiv \bar{J}_{n2,n5}$, $\bar{J}_{3''} \equiv \bar{J}_{n4,n6}$, and $\bar{J}_{3'''} \equiv \bar{J}_{n5,n9}$, where the $\bar{J}_1$ family occur along the hexagonal c-axis, the $\bar{J}_2$ family lie in the hexagonal plane, and the $\bar{J}_3$ family involve diagonal sites. In addition, the next-nearest-neighbor (nnn) interactions along the c-axis $\bar{J}_4 \equiv \bar{J}_{n1,n3}$, $\bar{J}_{4'} \equiv \bar{J}_{n2,n4}$, $\bar{J}_{4''} \equiv \bar{J}_{n8,n10}$ (with intervening cation present), and $\bar{J}_{4'''} \equiv \bar{J}_{n5,n6}$ (with intervening vacancy) will be considered.

We have used the generalized Luttinger-Tisza (GLT) method[8] to study the ground-state spin configurations in Cr_5S_6. In this method, the energy of Eq. (1) is minimized subject to the "weak" constraint that

$$\Sigma_{n\nu} \beta_\nu^{-2} \vec{S}_{n\nu} \cdot \vec{S}_{n\nu} = N \Sigma_\nu \beta_\nu^{-2} \quad , \qquad (2)$$

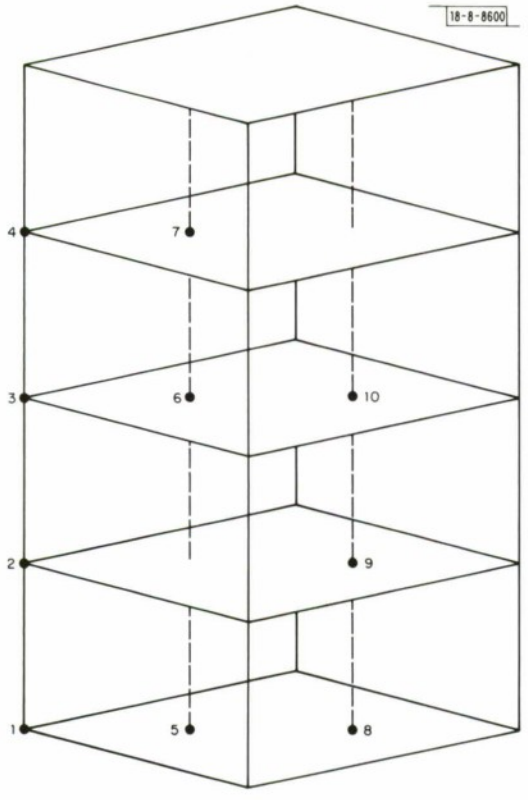

Fig. III-4. Cotion sites in unit cell of Cr_5S_6.

where the parameters β_ν are initially arbitrary, but are uniquely determined in the process of applying the method. The resulting minimum energy is given by

$$\mathcal{E} = E/(N\bar{J}_1) = \lambda_o \Sigma_\nu \beta_\nu^{-2} \quad , \tag{3}$$

where λ_o is the minimum eigenvalue – minimum over all branches and over all $\vec{k}$ in the first Brillouin zone – of the matrix function

$$L_{\nu\mu}(\vec{k}) = \beta_\nu \beta_\mu \Sigma_m (\bar{J}_{n\nu,\, m\mu}/\bar{J}_1) \exp[i\vec{k} \cdot (\vec{R}_{m\mu} - \vec{R}_{n\nu})] \quad , \tag{4}$$

where $(\vec{R}_{m\mu} - \vec{R}_{n\nu})$ is the vector separation of the interacting sites. It is often possible to choose the β_ν so that a physical spin configuration (one composed of unit spin vectors) can be constructed from some linear combination of degenerate eigenvectors associated with the minimum eigenvalue λ_o. Whenever this occurs, the GLT reasoning proves the resulting configuration to be the ground state.

When only nn interactions are considered, it appears that values can be found for the β_ν such that $L(\vec{k} = 0)$ always yields the ground state of Cr_5S_6. A map showing the different ground-state regions for a particular set of interaction relationships is given in Fig. III-5(a). The collinear configurations are constructed from a single eigenvector of L(0) and the canted configurations, from a linear combination of two degenerate eigenvectors. The boundaries between the different types of ground states in Fig. III-5(a) arise either from the onset of canting or from discontinuities in the canting angles caused by shifts from one eigenvalue branch to another. Differentiation

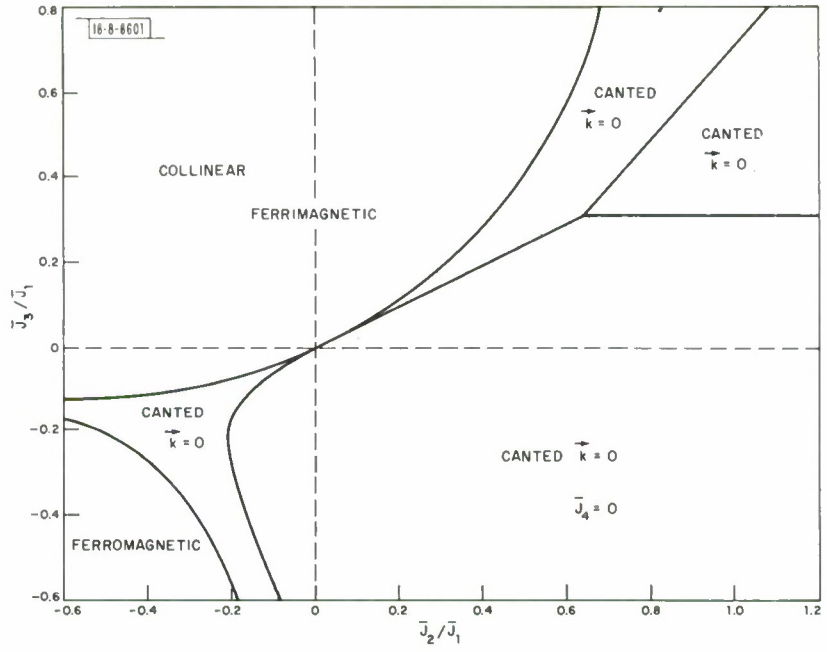

(a) Na next-nearest-neighbor interactions.

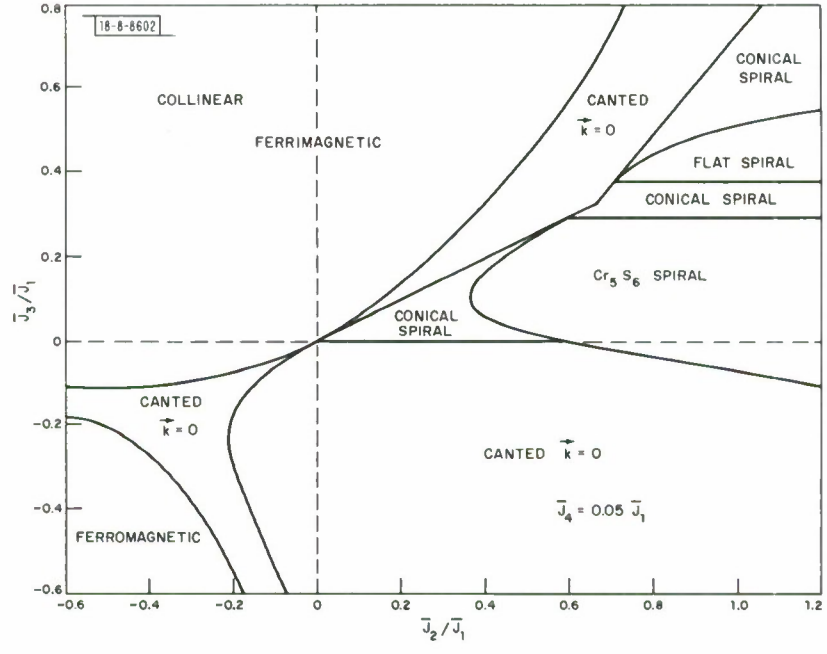

(b) $\bar{J}_4 = 0.05\ \bar{J}_1$.

Fig. III-5. Ground-state regions when all interactions within each family are equal.

among the vertical, horizontal, or diagonal interactions does not alter the topology of this map – it merely serves to weaken the discontinuities.

Because of the great flexibility of the canted $\vec{k} = 0$ configurations, nnn interactions must be introduced in order to obtain a spiral ground state. Once introduced, however, small values for the $\bar{J}_4$ interactions have a profound effect on the spin configurations. The value $\bar{J}_{4'''} = 0.01\,\bar{J}_1$ is sufficient to destabilize the canted $\vec{k} = 0$ configurations in the vicinity of the boundary shown at $\bar{J}_3 = 0.33\,\bar{J}_1$, $\bar{J}_2 > 0.6\,\bar{J}_1$ in Fig. III-5(a), although a somewhat larger value is required before a pure spiral of the type described by van Laar[9] becomes the ground state for any set of nn interactions.

A map of the ground-state regions for $\bar{J}_4 = \bar{J}_{4'} = \bar{J}_{4''} = \bar{J}_{4'''} = 0.05\,\bar{J}_1$ is presented in Fig. III-5(b) for the same set of nn interactions considered in Fig. III-5(a); a comparison of these two figures gives a dramatic demonstration of the effect of small nnn interactions. The general shape and location of the ground-state region of the Cr_5S_5-type spiral are not affected by variation of the nn interactions, although the boundaries shift somewhat. Consequently it appears probable that interactions of the $\bar{J}_3$ family are antiferromagnetic ($\bar{J}_3/\bar{J}_1 > 0$) and relatively weak ($\bar{J}_3 < \bar{J}_2 < \bar{J}_1$), contrary to van Laar's assumption. However, the length of the spiral propagation vector $\vec{k}_o$ is so sensitive to differentiation within the $\bar{J}_3$ and $\bar{J}_4$ families that comparison of van Laar's value with our ground-state calculations yields relatively little information about these interactions. We can only conclude that $0.3\,\bar{J}_1 < \bar{J}_{1'} < \bar{J}_1$, $\bar{J}_{2''} \approx 0.9\,\bar{J}_2$, $0 < \bar{J}_3$, etc. $< 0.2\,\bar{J}_1$, and $0.03\,\bar{J}_1 <$ at least one member of the $\bar{J}_4$ family $< 0.1\,\bar{J}_1$.

For finite temperatures, we turn to an investigation of the magnetic free energy, F_M, in the molecular-field approximation

$$F_M/\bar{J}_1 = \Sigma_{n\nu}\,\{\langle\vec{S}_{n\nu}\rangle \cdot \vec{H}'_{n\nu} - (kT/\bar{J}_1)\ln\sinh[(2S_\nu + 1)\,H'_{n\nu}\bar{J}_1/kTS_\nu] + (kT/\bar{J}_1)\ln\sinh[H'_{n\nu}\bar{J}_1/kTS_\nu]\}\quad , \tag{5}$$

where $\langle\vec{S}_{n\nu}\rangle$ is the thermal average of the spin vector $\vec{S}_{n\nu}\vec{H}'_{n\nu} = -\Sigma_{m\mu}(\bar{J}_{n\nu,m\mu}/\bar{J}_1)\langle\vec{S}_{m\nu}\rangle$. We have written a Fortran computer program which uses both the simplex and Newton-Raphson methods alternately to minimize this free energy, starting from a spiral ground state. We find that the phase angle and propagation vector both decrease with increasing temperature, and that they vanish at some $T_t < T_c$ provided that interactions of the $\bar{J}_4$ family are not too strong. The computed configuration above T_t is ferrimagnetic, in agreement with experiment, but the necessity for agreement with the observed value of $T_t \cong 0.5\,T_c$ further restricts the permissible range of interaction strengths. Thus it appears that $0.4\,\bar{J}_1 < \bar{J}_{1'} < 0.7\,\bar{J}_1$, $0.5\,\bar{J}_1 < \bar{J}_2 < \bar{J}_1$, $0.85\,\bar{J}_2 < \bar{J}_{2''} < \bar{J}_2$, $0 < \bar{J}_3$, etc., $< 0.1\,\bar{J}_1$, and the $\bar{J}_4$ family $= 0.05\,\bar{J}_1$.

K. Dwight
N. Menyuk

C. LASER SCATTERING

1. Two-Magnon Raman Scattering in K_2NiF_4

We have observed two-magnon Raman scattering from the antiferromagnet K_2NiF_4. This material has properties of a two-dimensional antiferromagnetic system, and the theoretical

Green's function calculation of the Raman spectrum was carried out for the quadratic-layer structure appropriate for K_2NiF_4. The experimental results at low temperature are consistent with the theory and give a nearest-neighbor intraplanar exchange constant $J = 77.0 \pm 2.0\,cm^{-1}$. This is in excellent agreement with the results of one-magnon neutron scattering experiments,[10] which gave $J = 78.2 \pm 0.3\,cm^{-1}$. The qualitative temperature dependence of the two-magnon Raman line was observed, and was also similar to the one-magnon scattering behavior.

S. R. Chinn
H. J. Zeiger
J. R. O'Connor

2. Raman Spectrum of Ti_2O_3

The Raman spectrum of Ti_2O_3 has been studied at temperatures from 1.7° to 800°K, using various excitation lines (4579 to 5145 Å) of an argon-ion laser. Seven Raman modes were observed by surface scattering (see Fig. III-6), namely, five E_g modes at 228, 302, 347, 452, 564 cm^{-1}, and two A_{1g} modes at 269 and 530 cm^{-1}, as predicted for D_{3d}^6 point group symmetry. A strong resonant enhancement of the E_g mode (228 cm^{-1}) intensity relative to the A_{1g} (269 cm^{-1}) mode intensity was observed for laser photon energies up to 2.71 eV (4579 Å). This is near the ϵ_2 peak at 2.8 eV obtained from reflectivity[11] data. The persistence of all Raman modes at high temperatures (up to 800°K) in this case implies no change of crystal symmetry above the semiconductor-metal transition observed[12] about 400°K. Figure III-7 presents the frequency and intensity relative to the other modes of the A_{1g} mode as a function of temperature. These changes are interpreted in terms of electronic and unit cell parameter changes on going through the semiconductor-metal transition. A more detailed account of the present work is presented elsewhere.

A. Mooradian
P. M. Raccah

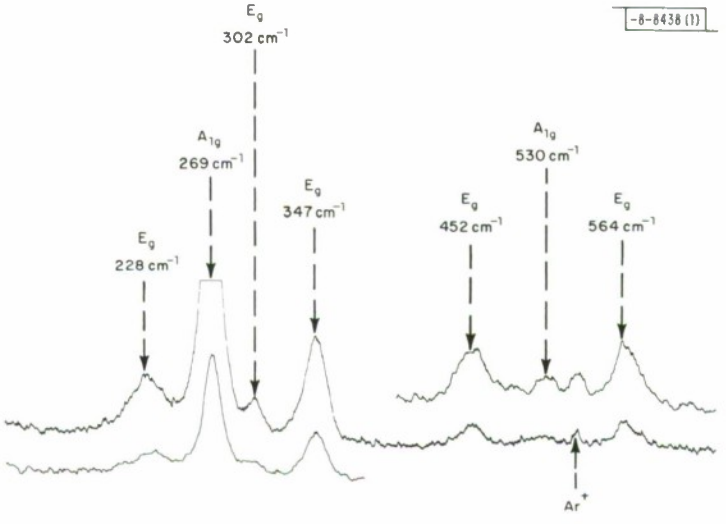

Fig. III-6. Raman spectrum of Ti_2O_3 at 300°K.

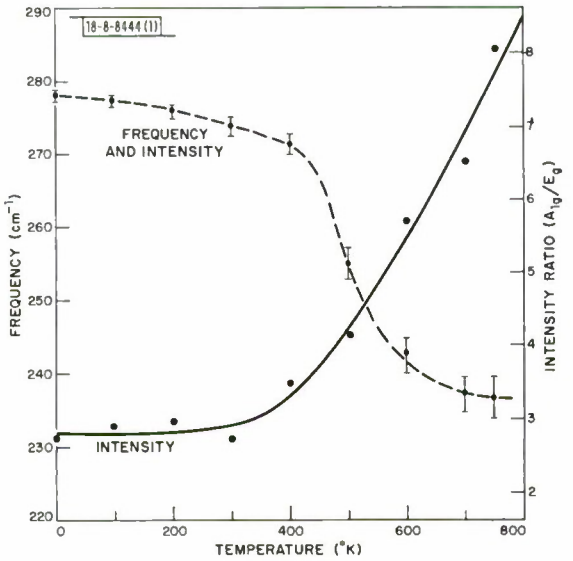

Fig. III-7. Frequency and intensity of A_{1g} mode in Ti_2O_3 os o function of temperature.

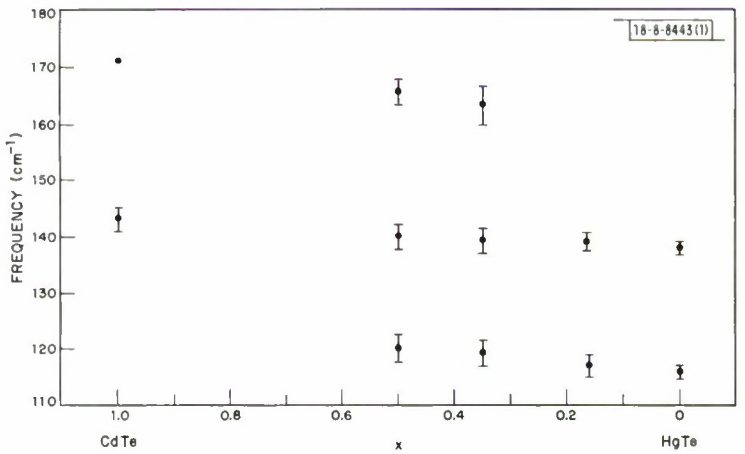

Fig. III-8. Optical phonon frequencies for various $Cd_xHg_{1-x}Te$ olloys ot 1.7°K.

3. Raman Scattering from $Hg_xCd_{1-x}Te$

Raman scattering from optical phonons in $Hg_xCd_{1-x}Te$ has been investigated for the range $0 \leqslant x < \underline{1}$. Surface scattering techniques were employed using an argon ion laser with sample temperatures between 300° and 1.7°K. The alloys exhibited scattering characteristic of a type II system where both the TO and LO phonon modes characteristic of those for pure CdTe (TO = 144 cm^{-1}, LO = 171 cm^{-1}) and pure HgTe (TO = 116 cm^{-1}, LO = 139 cm^{-1}) are present with intensities proportional to alloy composition. Figure III-8 shows the experimentally determined optical phonon frequencies for different alloy compositions. Strong resonant enhancement of the LO modes relative to the TO modes was observed for argon laser frequencies near the E_1 interband transition for HgTe and the $E_o + \Delta_o$ gap for CdTe. Figure III-9 gives the recorder traces for pure HgTe and pure CdTe. Multiple LO phonon overtone processes were also observed for CdTe for strongly resonant pumping similar to that reported for InAs[13] and CdS.[14] The strong resonant behavior of the LO modes greatly aided in discriminating against the modes of trigonal tellurium which occurred close to those for pure HgTe when the laser intensity was strong enough to decompose the samples' surface. No resonant enhancement of the trigonal modes was observed. A more extensive account of this work is published elsewhere.[15]

A. Mooradian
T. C. Harman

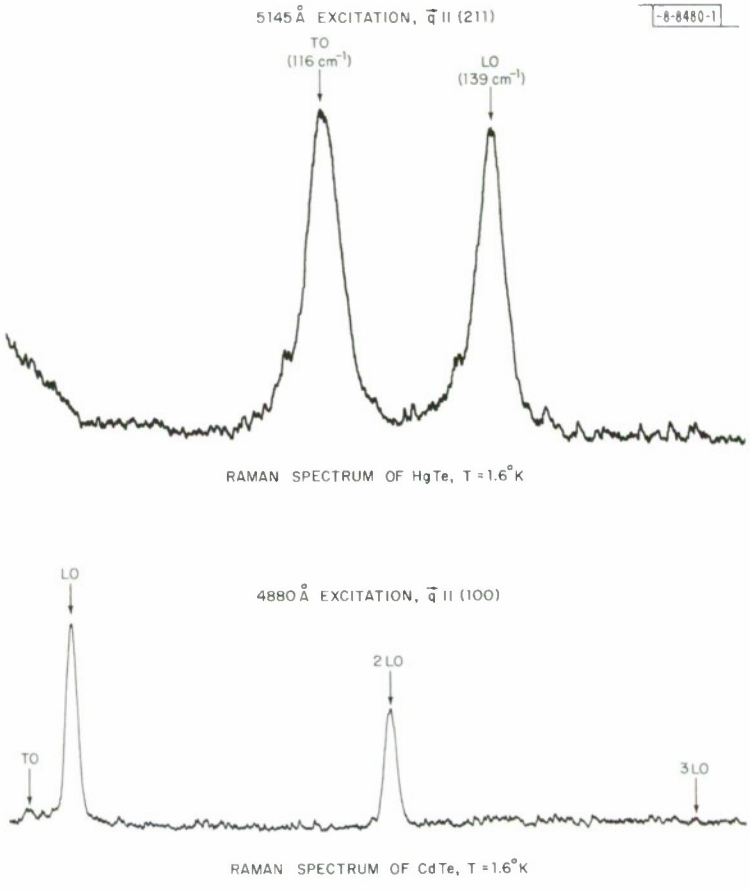

Fig. III-9. Recorder traces of Raman spectra of pure HgTe; (top) for 5145 Å excitation and pure CdTe; (bottom) for 4880 Å excitation at 1.7°K.

4. Light Scattering from Drifted Carriers in n-GaAs

The Raman spectrum of light scattered from single particle electron excitations in GaAs has been shown to be a direct measure of not only an equilibrium electron velocity distribution function[16] but of a nonequilibrium distribution when the momentum transfer is parallel to the field. A Q-switched 1.06-μ YAG:Nd laser was used to backscatter from drifted carriers in n-GaAs ($n < 10^{16}$ cm^{-3}) in pulsed electric fields up to the Gunn threshold. The geometry for scattering is shown in Fig. III-10. Voltage pulses 50-nsec wide were synchronized with 100-nsec laser pulses at up to 50 pulses/second. For lattice temperatures of 300°K, large increases in the electron velocities over thermal equilibrium were observed for fields in excess of 2000 V/cm. Figure III-11 shows spectra for GaAs with $n = 4 \times 10^{15}$ cm^{-3}. A detailed account of the present work is presented elsewhere.

A. Mooradian
A. G. Foyt

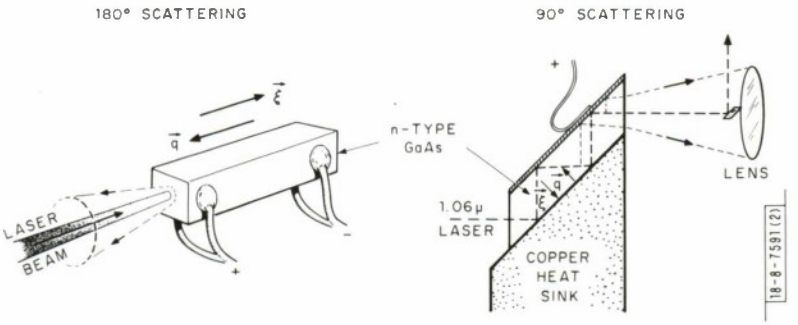

Fig. 10. Sample geometry used to scatter from drifted carriers.

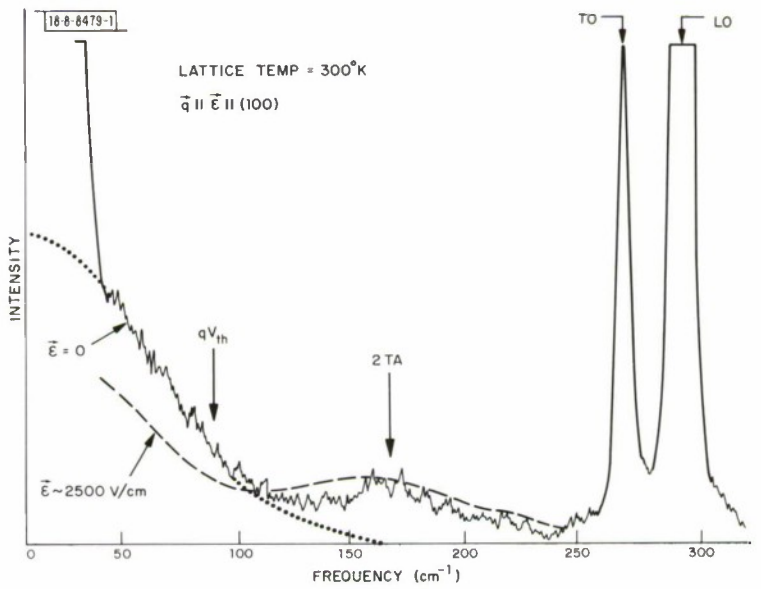

Fig. 11. Raman spectrum of GaAs ($n = 4 \times 10^{15}$ cm^{-3}) at 300°K in backscatter geometry. Incident and scattered light are parallel to electric field along (100) axes.

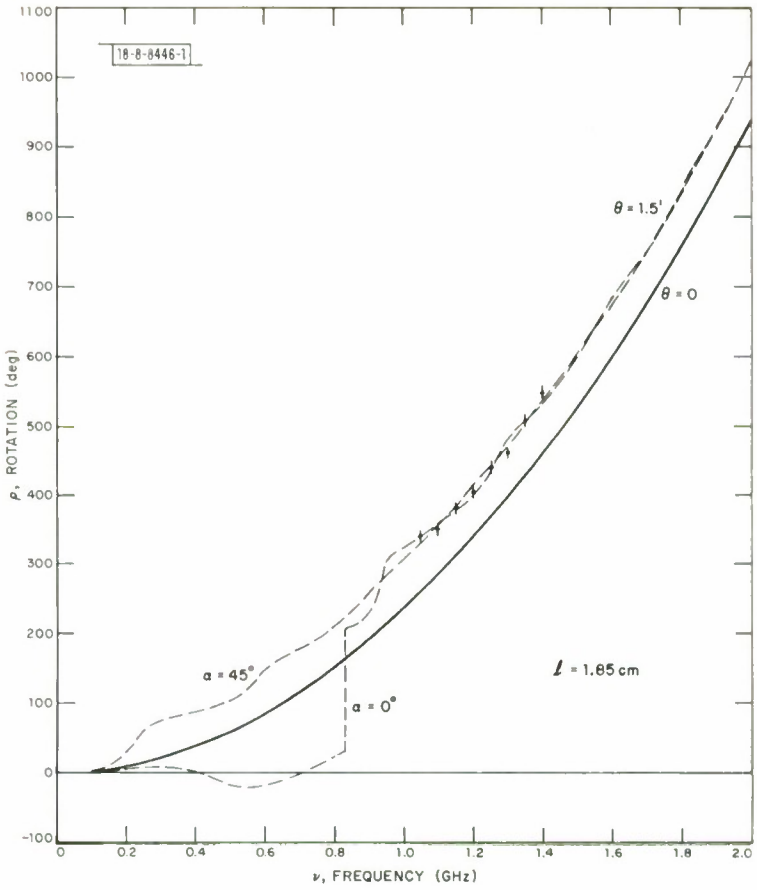

Fig. 12. Acousticol octivity in α-quartz: rotation dispersion in 1.85-cm crystal.

5. Acoustical Activity in α-Quartz

A rotation of the polarization of microwave frequency (1.05 to 1.40 GHz) shear waves propagating close to the optical axis in α-quartz has been observed. This constitutes the first direct ultrasonic measurement of the phenomenon of acoustical activity predicted by Portigal and Burstein.[17] The magnitude of the acoustical activity is in good agreement with that calculated from a recent Brillouin scattering determination of the linear wave-vector splitting of the two transverse acoustic normal modes. A very small misorientation of the surface normal to the c-axis ($\sim$ 1.5 arc minutes) strongly affects the rotation because of the presence of an anisotropic acoustical birefringence. However, the acoustical activity is easily sorted out from the birefringence, using the classical theories for the analogous problem in crystal optics. In Fig. III-12, the data are plotted and compared to the theoretical rotation for the perfectly oriented sample, $\Theta = 0$, and the off-axis sample, $\Theta = 1.5$ arc minutes. The sense of the rotation is opposite to that of the optical activity.

A. S. Pine

REFERENCES

1. R. Kubo, J. Phys. Soc. Japan 12, 570 (1957).
2. D. Pines, Elementary Excitations in Solids (W.A. Benjamin, Inc., New York, 1963).
3. J.J. Hopfield, Phys. Rev. 139, A419 (1965).
4. A.W. Overhauser, Phys. Rev. 156, 844 (1967).
5. J. des Cloizeaux, J. Phys. Rad. 20, 606 (1959).
6. W. Langer, M. Plischke and D. Mattis, Phys. Rev. Letters 23, 1448 (1969).
7. T.A. Kaplan, Bull. Am. Phys. Soc. 13, 386 (1968); T.A. Kaplan and P.N. Argyres, accepted for publication in Phys. Rev., March 1970; T.A. Kaplan and R.A. Bari, accepted for publication in J. Appl. Phys. Suppl. in 1970.
8. D.H. Lyons and T.A. Kaplan, Phys. Rev. 120, 1580 (1960).
9. B. van Laar, Phys. Rev. 156, 654 (1967).
10. R.G. Birgeneau, J. Skalyo, Jr. and G. Shirane, 15th Annual Conference on Magnetism and Magnetic Materials, Philadelphia, 1969.
11. W.J. Scouler and P.M. Raccah, Bull. Am. Phys. Soc. 15, 289 (1970); see also, contribution III-A-1 of this report.
12. C.N.R. Rao, R.E. Lochman and J.H. Honig, Phys. Letters 27A, 271 (1968).
13. K.W. Nill and A. Mooradian, Bull. Am. Phys. Soc. 13, 1658 (1968).
14. R.C.C. Leite, J.F. Scott and T.C. Damen, Phys. Rev. Letters 22, 780 (1969); M.V. Klein and S.P.S. Porto, ibid.
15. A. Mooradian and T.C. Harman, Proceedings of Conference on the Physics of Semimetals and Narrow Bandgap Semiconductors, Dallas, March, 1970 (to be published).
16. _____, Advances in Solid State Physics, Festkorperprobleme IX, O.E. Madelung, Ed. (Pergamon Press, New York, 1969) pp. 73-98.
17. D.L. Portigal and E. Burstein, Phys. Rev. 170, 673 (1968).

DOCUMENT CONTROL DATA – R&D

(Security classification of title, body of abstract and indexing annotation must be entered when the overall report is classified)

1. ORIGINATING ACTIVITY *(Corporate author)* Lincoln Laboratory, M.I.T.	2a. REPORT SECURITY CLASSIFICATION Unclassified 2b. GROUP None

3. REPORT TITLE

Solid State Research

4. DESCRIPTIVE NOTES *(Type of report and inclusive dates)*

Quarterly Technical Summary – 1 November 1969 through 31 January 1970

5. AUTHOR(S) *(Last name, first name, initial)*

McWhorter, Alan L.

6. REPORT DATE 15 February 1970	7a. TOTAL NO. OF PAGES 52	7b. NO. OF REFS 67
8a. CONTRACT OR GRANT NO. AF 19(628)-5167 b. PROJECT NO. 649L c. d.	9a. ORIGINATOR'S REPORT NUMBER(S) Solid State Research (1970:1) 9b. OTHER REPORT NO(S) *(Any other numbers that may be assigned this report)* ESD-TR-70-33	

10. AVAILABILITY/LIMITATION NOTICES

This document has been approved for public release and sale; its distribution is unlimited.

11. SUPPLEMENTARY NOTES None	12. SPONSORING MILITARY ACTIVITY Air Force Systems Command, USAF

13. ABSTRACT

This report covers in detail the solid state research work at Lincoln Laboratory for the period 1 November 1969 through 31 January 1970. The topics covered are Solid State Device Research, Materials Research, and Physics of Solids.

14. KEY WORDS

solid state devices
materials research
magnetism
Raman scattering
infrared
crystal growth
x-ray scattering
laser scattering
electronic band structure
magneto-optical research
Brillouin scattering
magnetic semiconductors